HELSINKI UNIVERSITY OF TECHNOLOGY
Faculty of Electronics, Communications and Automation

Juhamatti Nikander

Induction Motor Parameter Identification in Elevator Drive Modernization

Thesis submitted for examination for the degree of Master of Science in Technology

Espoo 7.1.2009

Thesis supervisor:

Prof. Jorma Luomi

Thesis instructor:

M.Sc. Lauri Stolt

Author: Juhamatti Nikander

Title: Induction Motor Parameter Identification in Elevator Drive Modernization

Date: 7.1.2009 Language: English Number of pages: 10+68

Faculty: Faculty of Electronics, Communications and Automation

Professorship: Electric Drives Code: S-81

Supervisor: Prof. Jorma Luomi

Instructor: M.Sc. Lauri Stolt

A study is presented where an induction motor, whose rotor is not allowed to rotate, is identified using system identification methods based on transient and frequency response tests. Precise control of elevators powered with frequency converter fed induction motors depends on the accuracy of the parameters used in the motor controller, particularly when no external position or speed sensors are used. When an elevator is modernized with a new control system, the old motor cannot be identified with a regular locked rotor and no-load tests as the motor is not allowed to rotate. However, the identification can be performed in such conditions by analyzing the voltages and currents when the motor windings are excited with such an AC or DC that does not produce torque. A step response method is introduced for the DC excitation where the desired motor parameters are obtained as a result when the measured data is processed with state variable filters, and the produced linear system of equations is solved with a recursive least-squares algorithm. The frequency response method presented uses both DC and AC excitation. The method is based on finding the amplitude ratio and the phase difference between the voltage and current phasors using the properties of the Fourier series. This information is then used to calculate the inductance between the motor terminals, from which the other motor parameters can be solved. Both methods are tested with simulations and experiments. The final choice of the proper identification method is found to be a compromise between the parameter accuracy and measurement time.

Keywords: Elevator, induction motor, self-commissioning, parameter identification, standstill, step response, frequency response, state variable filtering, recursive least-squares

TEKNILLINEN KORKEAKOULU

DIPLOMITYÖN TIIVISTELMÄ

Tekijä: Juhamatti Nikander

Työn nimi: Oikosulkumoottorin parametrien identifionti hissikäytön modernisoinnissa

Päivämäärä: 7.1.2009 Kieli: Englanti Sivumäärä: 10+68

Tiedekunta: Elektroniikan, tietoliikenteen ja automaation tiedekunta

Professuuri: Sähkökäytöt Koodi: S-81

Valvoja: Prof. Jorma Luomi

Ohjaaja: Dipl.Ins. Lauri Stolt

Tässä työssä tutkitaan, miten oikosulkumoottorin sähköiset parametrit voidaan identifioida askel- ja taajuusvastemenetelmien avulla pyörittämättä roottoria. Oikosulkumoottoria voimanlähteenä käyttävien hissien ohjaustarkkuus riippuu pitkälti siitä, miten tarkasti taajuusmuuttajan momentti- ja nopeussäätäjän parametrit vastaavat todellisia varsinkin, jos hissin paikkaa tai nopeutta ei mitata. Vanhojen hissien modernisoinnin yhteydessä ongelmaksi muodostuu se, että olemassa olevaa moottoria ei voi identifioida perinteisillä oikosulku- ja tyhjäkäyntikokeilla, koska moottoria ei voi pyörittää kuormattomana. Sen sijaan identifiointi voidaan tehdä analysoimalla vaihejännitteitä ja -virtoja, joita esiintyy, kun staattorikäämityksiin syötetään sellainen heräte, joka ei aiheuta pyörivää sähkömagneettista kenttää eikä siten vääntömomenttia. Esitettävässä askelvastemenetelmässä moottoria syötetään tasavirtapulsseilla, jolloin halutut parametrit saadaan, kun vaihejänniteen ja -virran mittaukset prosessoidaan tilamuuttujien suodatuksella ja saatu lineaarinen yhtälöryhmä ratkaistaan rekursiivisella pienimmän neliösumman algoritmilla. Toisessa, taajuusvasteeseen perustuvassa, menetelmässä moottoria syötetään yhtä aikaa sekä tasa- että vaihtovirralla. Tällöin moottorin parametrit voidaan ratkaista vaihejännitteen ja -virran välisen amplitudisuhteen ja vaihe-eron perusteella lasketun moottorin liittimistä näkyvän induktanssin taajuusriippuvuuden avulla. Molempia menetelmiä on tutkittu sekä tietokonesimuloinneilla että kokeellisilla menetelmillä. Tulosten perusteella havaittiin valitun menetelmän olevan kompromissi parametrien tarkkuuden ja testin suoritusajan välillä.

Avainsanat: Hissikäyttö, oikosulkumoottori, parametrien identifiointi, askelvaste, taajuusvaste, tilamuuttujien suodatus, rekursiivinen pienin neliösumma

Acknowledgements

This Master's thesis has been carried out for the R&D drive team of the elevator corporation Kone at Hyvinkää, Finland. I would like to thank the team leader, Jari Helvilä, for providing this challenging and interesting subject available, and the chief design engineer, Tuukka Kauppinen, for bringing this subject to my attention.

I wish to express my gratitude to the personnel in the Electric Drives Group of Helsinki University of Technology: my supervisor, Professor Jorma Luomi, for the substantial guidance and support given in scientific writing, and for the valuable opinions expressed during the year. Special thanks go to Dr. Marko Hinkkanen for providing initial literature on the subject, and for pointing out valuable comments.

I want to thank my instructor, M.Sc. Lauri Stolt, for the interest shown towards the subject and for the practical tips given in the many educational discussions we had. I also appreciated the support provided on programming, proofreading and teaching drive electronics.

I would also like to thank the drive specialists, Esa Putkinen, Risto Jokinen and Pekka Hytti, for the professional comments and advice given regarding electronics used in elevator drives. Furthermore, I wish to thank the other members of the drive team and other people at Kone not mentioned here for providing the most friendly working environment.

Finally, I would like to thank my family for the love and support they have been giving during the years of my studies.

Otaniemi, 7.1.2009

Juhamatti Nikander

Contents

Abstract ii

Abstract (in Finnish) iii

Acknowledgements iv

Contents v

Symbols and Abbreviations vii

1 Introduction 1

1.1 Objectives and Scope . . . 2

1.2 Structure . . . 3

2 Elevator Drive 4

2.1 Elevator Mechanics . . . 4

2.2 Frequency Converter . . . 6

3 Induction Motor Theory 11

3.1 Structure and Operating Principle . . . 11

3.2 Electrical Model . . . 12

3.3 Mechanical Model . . . 17

4 Motor Control 18

4.1 Rotor Field Orientation . . . 19

4.2 Controller Detuning Effects . . . 20

5 Motor Identification Methods 22

5.1 Motor Name-plate . . . 22

5.2 Stator Resistance Measurement . . . 25

5.3 Locked Rotor and No-load Tests . . . 27

5.4 Standstill Identification . . . 30

5.5 Literature Review on Standstill Identification Methods . . . 35

5.6 Step Response Identification . . . 37

5.7 Identification with State Variable Filtering . . . 40

5.8 Frequency Response Identification 44
5.9 Magnetizing Curve Identification 48

6 Simulation Results **51**

7 Experimental Results **57**

8 Conclusions **60**

References **62**

A Linear Regression **67**

Symbols and Abbreviations

a_i, b_i	coefficients of ith terms in polynomials $U(s)$ and $Y(s)$
B	viscous damping coefficient
B_e	B of the motor shaft
B_l	B of the load reduced to the secondary wheel
f_0	low-pass filter cut-off frequency
f_1	stator frequency
f_2	slip frequency
f_s	sampling frequency
f_{sw}	switching frequency
g_i	intermediate result in RLS algorithm
h	sampling period
$\mathbf{I}$	identity matrix
I_{ac}	alternating current
I_{dc}	direct current
I_{s0}	stator no-load current
i_{mec}	gear transmission ratio
J_e	inertia of the motor shaft
J_l	inertia of the load reduced to the secondary wheel
k	discrete time unit
K_l	torsional spring coefficients reduced to the secondary wheel
$K(\omega_1)$	system gain
l	number of cycles measured during t_m
L_D	dynamic magnetizing (mutual) inductance
L_e	effective stator inductance
L_m	magnetizing (mutual) inductance
L_M	transformed magnetizing (mutual) inductance
L_r, L_s	rotor and stator self-inductances
$L_{r\sigma}$, $L_{s\sigma}$	rotor and stator leakage inductances
L_σ	total leakage inductance
m_a, m_f	amplitude and frequency modulation ratios
N	number of measurement points
p	number of pole pairs
$\mathbf{P}$	covariance matrix
P_{Cur}, P_{Cus}	resistive power losses in rotor and stator
P_{Fer}, P_{Fes}	iron losses in rotor and stator
P_{fr}	friction losses
p_{ij}	element in $\mathbf{P}$ on ith row and jth column
P_{in}	active three-phase input power
P_{in0}, P_{ink}	no-load and short-circuit input powers
P_{out}	mechanical output power
P_{str}	stray losses
P_{wi}	windage losses
Q_0	no-load Q_{in}

Q_{in}	reactive three-phase input power
Q_M	reactive power consumed in L_M
Q_σ	reactive power consumed in L_σ
R_{ab}, R_{bc}, R_{ca}	resistances between two stator terminals a, b or c
R_D	dynamic resistance
R_e, R_{ei}	effective stator resistance with and without inverter nonlinearity
R_{Fe}	core loss resistance
R_i	inverter resistance
R_r, R_s	rotor and stator resistances
R_R	transformed rotor resistance
R_{sk}	short-circuit stator resistance
$R_{s,\mathrm{Y}}$, $R_{s,\Delta}$	stator resistances in Y and Δ connected motors
s	Laplace variable
S_{in}	apparent three-phase input power
S_{in0}, S_{ink}	no-load and short-circuit S_{in}
t	time
t_1	period of f_1
t_a, t_b, κ	transistor turn-off parameters
t_{ct}	time duration of IGBT's tail current
t_d	inverter dead-time
$t_{d,on}$, $t_{d,off}$	time delays in transistor base drive turn-on and turn-off
$t_{d,swon}$	transistor switch-on delay time
T_e	electrical torque
T_{fr}	friction torque
T_l	load torque
t_m	measurement time
t_{on}, t_{off}	transistor turn-on and turn-off times
t_r, t_f	rise and fall times
t_{sw}	switching period
$\mathbf{U}$	input vector
U_{dc}	voltage over filter capacitor
u_f, y_f	filter input and output
$U(s)$, $Y(s)$	Laplace transformed $u(t)$ and $y(t)$
U_{s0}, U_{sk}	no-load and short-circuit stator voltages
u_{si}	stator voltage in phase i
$U(\lambda)$, $Y(\lambda)$	$U(s)$ and $Y(s)$ with λ notation
X_M	transformed magnetizing reactance
$X_{r\sigma}$, $X_{s\sigma}$	rotor and stator leakage reactances
X_{sk}	short-circuit stator reactance
X_σ	total leakage reactance
$\mathbf{Y}$	output vector
Z_M	transformed magnetizing impedance
Z_s	stator impedance
Z_{s0}, Z_{sk}	no-load and short-circuit stator impedances
α	covariance matrix gain

α_i, β_i	coefficients of ith terms in polynomials $U(\lambda)$ and $Y(\lambda)$
$\boldsymbol{\gamma}$	update coefficient vector
γ_i	update coefficient of ith parameter
δ_1	angle between real axes of phase a and synchronous frame d
δ_r	rotor angle
η_g	gear efficiency when power flows to the motor
η_m	gear efficiency when power flows to the load
$\boldsymbol{\theta}$	parameter vector
θ_i	ith model parameter
λ	Lambda operator
μ	forgetting factor
σ	leakage factor
τ_m	mechanical time constant
τ_r, τ_s	rotor and stator time constants
τ'_s	transient stator time constant
$\boldsymbol{\varphi}$	regression vector
$\boldsymbol{\Phi}$	regression matrix
φ_0, φ_k	angle φ_1 in no-load and short-circuit conditions
φ_1	angle between stator voltage and current phasors
ω_0	filter angular cut-off frequency
ω_1	stator angular frequency
ω_2	rotor (slip) angular frequency
Ω_l	angular speed of the load
ω_r	electrical angular speed of the rotor
Ω_r	mechanical angular speed of the rotor

Space Vectors

$\underline{i}_0$	no-load magnetizing current
$\underline{i}_{Fe}$	iron loss current
$\underline{i}_m$	magnetizing current
$\underline{i}_M$	transformed magnetizing current
$\underline{i}_r$, $\underline{i}_s$	rotor and stator currents
$\underline{i}_R$	transformed rotor current
$\underline{u}_i$	inverter voltage drop
$\underline{u}_s$	stator voltage
$\underline{u}_{s,ref}$	reference stator voltage
$\underline{\psi}_m$	main flux linkage
$\underline{\psi}_r$, $\underline{\psi}_s$	rotor and stator flux linkages
$\underline{\psi}_{r\sigma}$, $\underline{\psi}_{s\sigma}$	rotor and stator leakage flux linkages
$\underline{\psi}_R$	transformed rotor flux linkage
$\underline{\psi}_\sigma$	total leakage flux linkage

Subscripts

a, b, c	phase a, b or c
d	real part in synchronous reference frame
N	nominal value
q	imaginary part in synchronous reference frame
r	rotor quantity
s	stator quantity
α	real part in stator reference frame
β	imaginary part in stator reference frame

Other Notations

$\underline{x}$	complex phasor or space vector
$\dot{x}$	derivative of x with respect to time
$\hat{x}$	amplitude of x
$\widehat{x}$	estimate or measurement of x
$\mathbf{x}$	vector
$\mathbf{X}$	matrix
X	root-mean-square quantity of x
$X(s)$	transfer function
Δx	difference $x_{i+1} - x_i$
$[\lambda^i x](t)$	i times filtered $x(t)$
$\lfloor x \rfloor$	the value of x rounded down to the closest integer

Abbreviations

AC	alternating current
CMFR	correlation method of frequency response
DC	direct current
DTC	direct torque control
IGBT	insulated gate bipolar transistor
FD	frequency domain
FIR	finite impulse response
FR	frequency response
IIR	infinite impulse response
LRNL	locked rotor and no-load
LS	least-squares algorithm
PI	proportional-integral
RLS	recursive least-squares
RMS	root-mean-square
SR	step response
SSFR	standstill frequency response
SVF	state variable filtering
TD	time domain

1 Introduction

Three-phase induction motors have been used widely in elevator applications for decades thanks to the motor's relatively simple structure, maintenance free operation and ability to start directly from the supply network. However, such an on-line starting consumes energy more than necessary, and the starts and stops become jerky as the motor can only be controlled with switches and relays.

During the 1980s, analog motor control systems evolved, and frequency converters became popular, enabling the use of drives with variable voltage and frequency, which improved the stopping accuracy of the elevator car and reduced overall energy consumption. Ever since the microprocessors became available with reasonable prices in the 1990s, the scope has been on controlling the motor more smoothly and efficiently.

Recently, the first generation of elevators with drives using induction motors have begun to reach the end of their lifespan increasing the market for elevator modernization. The idea is to replace the old and excessively worn parts of the drive with new high-performance and high-efficiency components while trying to keep the old motor and gear in place to avoid increasing the costs too much.

However, the name-plates of the old, as well as the new, induction motors have insufficient information, if any, to be used with modern control methods. In addition, the motors used in elevator installations are most likely to be supplied by various manufacturers instead of being built by the one modernizing the elevator. In such a case, a custom setup has to be carried out for the motor and drive electronics, which is a very time-consuming task and can only be performed by very experienced personnel. Therefore, there is a need for a drive capable of self-commissioning, i.e. identifying the parameters of an unknown motor without user intervention.

Previously, induction motors have been identified by performing several tests during which the rotor had to be kept locked mechanically or disconnected from the load, i.e. with the DC test, locked rotor test and no-load test. These restrictions cause problems in elevator modernization for several reasons. Although the rotor could be locked mechanically with the motor brakes, there is no guarantee that the old brakes will be able to hold the full pull-up torque produced in the locked rotor test in addition to the torque caused by the load - the unbalanced elevator car and counterweight. Of course, the torque could be produced into the direction opposite to the one caused by the load, or the system could be balanced by adding weighs either to the elevator car or to the counterweight. However, the system would still have to be modified for the no-load test.

A better idea would be to remove the heavy flywheel from the motor shaft and the mechanical coupling between the motor and the gear. However, the coupling cannot be removed without removing the brake arms, and doing so would cause the counterweight to fall freely. Thus, it would be first necessary to remove the ropes from the traction sheave, a grooved pulley connected to the secondary wheel of the gear, but the ropes, in turn, cannot be removed without lowering the counterweight

to the bumper and without locking the elevator car. Thus, there is no practical way of achieving the no-load conditions in any reasonable time.

1.1 Objectives and Scope

The objective of this Master's thesis is to find the most suitable identification method for the electrical parameters of a typical induction motor used in elevator applications. The following restrictions must be obeyed:

- The rotor is not allowed to rotate nor produce torque.
- The motor is supplied with a frequency converter where the stator voltages are not measured.
- The existing hardware must not be changed.
- The parameters should be accurate enough to be used in a modern speed sensorless vector control.

Luckily, the electrical parameters can be identified without rotating the motor at all if the stator windings are fed with an excitation that does not produce a rotating electromagnetic field, i.e. if the motor is controlled as if two of the three stator phases were connected to the frequency converter and the third one left connected, or as if the two phases were connected in parallel, and the resulting equivalent winding in series with the third one. With such an excitation, no torque is produced, and there is no need to lock the rotor nor disconnect the load.

Unfortunately, this type of standstill identification is not a very easy task to do as the identified system is far from being ideal due to the nonlinearities present in the frequency converter and in the induction motor itself. For example, the frequency converter's output voltage depends nonlinearly on the motor's phase currents because dead-time is added to the transistor switch-on delays. Moreover, the output voltage depends on the forward voltage drops of the used power devices, particularly when the output voltage is low. On the other hand, inductances formed by the stator windings and the rest of the magnetic circuit depend on the direction and the magnitude of the current due to hysteresis and saturation. Furthermore, the rotor resistance and leakage inductance change with stator frequency due to the skin and proximity effects. In addition, the iron losses dissipated in the motor core depend on that frequency.

The studied identification methods are divided into step and frequency response methods. In the former, the stator windings are supplied with either voltage or current steps, and the resulting current or voltage is measured, after which the measured data is fitted to the one calculated from the motor model. The fitting becomes possible if at least two measurements are gathered. In practice, the data is fitted with linear regression, reducing the effects of noise and single wrong measurements.

As a result, a parameter vector is obtained, from which the motor parameters can be calculated.

In the frequency response methods, the stator windings are supplied with sinusoidal voltages of constant amplitudes and frequencies. Furthermore, a DC current is used to set the correct level of magnetization and to reduce the effect of hysteresis. The measurements are taken from the current response after the initial transients have decayed. The idea is to calculate the amplitude ratio and phase difference between the fundamental voltage and current phasors. This information is then used to calculate the effective input inductance seen from the motor terminals at the frequencies of interest, after which the other motor parameters can be calculated from that inductance.

1.2 Structure

The contents of this thesis are organized in the following way. After this introduction, the following two chapters, 2 and 3, introduce mathematical models for a simple elevator, frequency converter and induction motor. In Chapter 4, motor control based on space vector theory is briefly reviewed, after which controller detuning effects are discussed.

The main subject of this thesis begins in Chapter 5 where the first section explains information that can be derived from the motor name-plate, and the second section discusses the problems that occur when winding resistances are measured with a frequency converter. Then, the locked rotor and no-load tests are presented, followed by a derivation of the model used in standstill identification. A literature review is presented in the middle of the chapter, and the remaining parts show how the motor is identified using the step and frequency response methods.

In the next two chapters, 6 and 7, different identification methods are studied with computer simulations and experimental tests. Finally, the thesis is concluded in Chapter 8.

2 Elevator Drive

The first section of this chapter describes a construction of a simple elevator and introduces a mathematical model for the mechanical dynamics, after which the structure and behavior of the elevator power supply, a frequency converter, is explained.

2.1 Elevator Mechanics

A simple elevator consists of a shaft, car, counterweight, ropes, a number of traction sheaves: pulleys with multiple grooves; bumpers, a motor and, possibly, a reduction gear, and necessary safety equipment. The shaft has guide rails on the walls, along which the car and the counterweight move vertically. Usually, the motor lies in its own machine room at the top of the shaft. The motor shaft is connected to the reduction gear or directly to the driving traction sheave, whose purpose, in addition to transforming rotation to transversal motion, is to add more friction to the ropes. The shaft, car and counterweight all have a number of deflector sheaves, whose purpose is to pass the ropes, connecting the car and counterweight along the sheaves, to a particular direction. With multiple ropes and deflector sheaves, forces acting on individual ropes can be reduced. The amount of this reduction is characterized by the roping factor. Any other roping than 1:1 causes the ropes to move faster than the elevator car. Therefore, the roping as well acts as a gear. The bumpers are placed at the bottom of the shaft, where they act as ultimate boundaries, against which the car and the counterweight will be stopped if other safety equipment fail to operate.

Dynamic Model

Modeling mechanical elevator dynamics is a very difficult task as the real elevator system has a vast number of moving parts with unknown parameters. However, a simple dynamic model can be built for simulation and model parameter verification purposes. The considered system in Figure 2.1 consists of two moments of inertia – one inertia J_e for the motor shaft and the other J_l for the rest of the moving elevator parts – connected to each other with a reduction gear. Frictions in the motor and gear, and the elevator are modeled with two viscous dampers B_e and B_l, respectively, and the oscillatory behavior, caused by the flexible ropes, with one torsional spring constant K_l. The gear is thought to be ideal, i.e. no backlash and unity efficiency. As such, the equations of motion are

$$J_e \frac{\mathrm{d}\Omega_1(t)}{\mathrm{d}t} = T_e(t) - B_e\Omega_1(t) - T_1(t) \tag{2.1a}$$

$$\frac{\mathrm{d}T_2(t)}{\mathrm{d}t} = K_l\Big[\Omega_2(t) - \Omega_l(t)\Big] \tag{2.1b}$$

$$J_l \frac{\mathrm{d}\Omega_l(t)}{\mathrm{d}t} = T_2(t) - B_l\Omega_l(t) - T_l(t) \tag{2.1c}$$

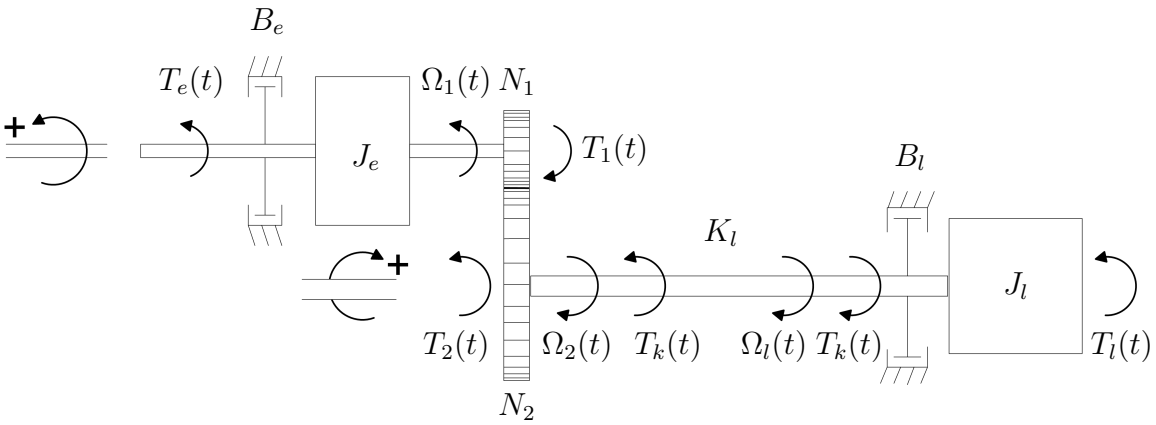

Figure 2.1: The two-inertia model of a simple elevator.

where $T_e(t)$ is the electrical torque produced by the motor, $T_1(t)$ the load torque reflected back through the gears, $T_2(t)$ the torque at the the imaginary shaft and $T_l(t)$ the load torque caused by the elevator. The variables $\Omega_1(t)$, $\Omega_2(t)$ and $\Omega_l(t)$ are the angular speeds of the primary wheel, secondary wheel and the load, respectively.

Gears

A gear has a transmission ratio i_{mec} defined as the inverse of the ratio of the applied torque T_1 to the transmitted torque T_2. This number is equal to the ratio of the numbers of teeth in respective wheels

$$i_{mec} = \frac{T_2}{T_1} = \frac{N_2}{N_1} = \frac{r_2}{r_1} \tag{2.2}$$

where N_1 and N_2 are the numbers of teeth and r_1 and r_2 the radii of the primary and secondary wheels, respectively. The latter equality holds as the circumference of a circle is directly proportional to its radius ($l = 2\pi r$). As the circumferences of the wheels travel equal distances in the same time, i.e. there is no slip ($v_1 = v_2$), there exists another expression for the transmission ratio

$$i_{mec} = \frac{\vartheta_1}{\vartheta_2} = \frac{\Omega_1}{\Omega_2} = \frac{n_1}{n_2}, \qquad (\vartheta_1 r_1 = \vartheta_2 r_2)\,, \tag{2.3}$$

where ϑ's, Ω's and n's are the angular displacements, angular speeds and rotational speeds of the respective wheels.

From the law of conservation of energy, the gear efficiency η_m can be calculated as

$$\eta_m = \frac{P_1 - P_{fr}}{P_1} = \frac{P_2}{P_1} = \frac{T_2\Omega_2}{T_1\Omega_1} = \frac{T_2}{T_1} \cdot \frac{1}{i_{mec}}, \qquad P_1 > P_2, \tag{2.4}$$

where P_1 and P_2 are the gear input and output powers, respectively, i.e. the power flows from the motor to the load. The power P_{fr} represents gear losses. When power

flows from the load to the motor, the latter working as a generator, the efficiency η_g is defined as

$$\eta_g = \frac{P_2 - P_{fr}}{P_2} = \frac{P_1}{P_2} = \frac{T_1\Omega_1}{T_2\Omega_2} = \frac{T_1}{T_2} i_{mec}, \qquad P_1 < P_2. \tag{2.5}$$

With the gear transmission ratio defined above, and noting that $T_1 = T_e$ and $\Omega_1 = \Omega_r$, the variables T_1, T_2, Ω_1 and Ω_2 can be removed from Equation (2.1) yielding a state space form

$$\begin{aligned}\dot{\mathbf{x}}_\mathbf{1}(t) &= \begin{bmatrix}\dot{\Omega}_r(t)\\ \dot{T}_e(t)\\ \dot{\Omega}_l(t)\end{bmatrix} = \begin{bmatrix}-B_e/J_e & -1/J_e & 0\\ K_l/i_{mec}^2 & 0 & -K_l/i_{mec}\\ 0 & i_{mec}/J_l & -B_l/J_l\end{bmatrix}\begin{bmatrix}\Omega_r(t)\\ T_e(t)\\ \Omega_l(t)\end{bmatrix} + \begin{bmatrix}1/J_e & 0\\ 0 & 0\\ 0 & -1/J_l\end{bmatrix}\begin{bmatrix}T_e(t)\\ T_l(t)\end{bmatrix}\\ &= \mathbf{A_1}\mathbf{x_1}(t) + \mathbf{B_1}\mathbf{u_1}(t).\end{aligned} \tag{2.6}$$

For control purposes, the actual use of this model is rather limited as it involves measuring the torque and the angular speed of the primary shaft with an expensive torque sensor and a tachometer. Therefore, the main purpose of this model is to simulate the pulsating load torque caused by flexible ropes.

For better dynamics, the model could be extended with less simplified elevator dynamics containing two dynamic masses for modeling the inertia of the car, counterweight and ropes and two viscous dampers and linear springs for modeling the flexibility of the ropes and other two viscous dampers for the car and counterweight. This less simplified model yields a fifth- to seventh-order model for the elevator dynamics and a third-order model for the motor dynamics. This thesis considers only the motor part. For more detailed modeling of elevator mechanics, the interested readers could refer to the Master's thesis by Salomäki (2003) and its references.

2.2 Frequency Converter

A frequency converter is a power electronics device that converts power from a supply network to a load with controllable amplitude and frequency. A schematic diagram of one topology of frequency converters used in elevator drives is shown in Figure 2.2. It consists of a three-phase, six-pulse, full-bridge diode rectifier (1), a brake chopper (2), a large filter capacitor (3) and a three-phase pulse-width-modulated voltage-source inverter (4). Measurements are taken from the voltage over the filter capacitor and from the currents of two output phases.

The first part rectifies the supply AC voltage into DC over the filter capacitor with the voltage given on average by

$$U_{dc} = \frac{3}{\pi}\sqrt{2}U_n \approx 1.35 \cdot U_n \tag{2.7}$$

where U_n is the supply network phase-to-phase voltage (Mohan et al., 2003). Due to the finite interval needed by current commutation between the conducting diodes,

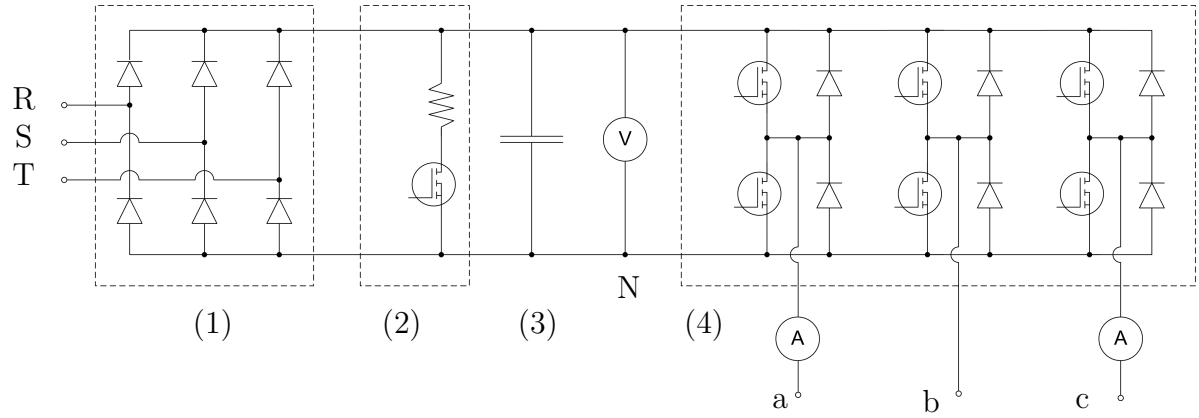

Figure 2.2: A typical frequency converter.

the DC side voltage (2.7) is reduced by

$$\Delta U_{dc} = \frac{3}{\pi}\omega_n L_k I_{dc} = 6 f_n L_k I_{dc} \tag{2.8}$$

where $\omega_n = 2\pi f_n$ is the angular frequency of the supply and L_k the short-circuit inductance of the supply network at the frequency converter's input terminals. The current I_{dc} is the current on the DC side.

The brake chopper is used to avoid voltage increase in the filter capacitor by dissipating the excess energy in the braking resistors when the power flows from the load to the supply, i.e. when the motor is braking or acting as a generator, and when the frequency converter is equipped with a diode-rectifier, which is not capable of converting this energy back to the supply.

The purpose of the PWM inverter is to create voltages with controllable magnitude and frequency. The inverter consists of three 'legs', each having two pairs of transistors and diodes, the upper and lower ones. The transistors in each one of these inverter-legs are controlled in a complementary fashion, i.e. one transistor conducts at a time, to avoid short-circuiting the filter capacitor.

The instantaneous inverter output voltages with respect to the assumed three-phase load neutral point are

$$u_{sa} = \frac{2}{3}u_{aN} - \frac{1}{3}\left(u_{bN} + u_{cN}\right) \tag{2.9a}$$

$$u_{sb} = \frac{2}{3}u_{bN} - \frac{1}{3}\left(u_{aN} + u_{cN}\right) \tag{2.9b}$$

$$u_{sc} = \frac{2}{3}u_{cN} - \frac{1}{3}\left(u_{aN} + u_{bN}\right) \tag{2.9c}$$

where $u_{iN}, i \in \{a, b, c\}$, are the amplitudes of the inverter output voltages with respect to the negative DC-bus.

When pulse-width modulation based on suboscillation method is used, the average inverter output voltage and frequency are characterized by the amplitude and

frequency modulation ratios m_a and m_f, respectively,

$$m_a = \frac{\hat{u}_{ctrl}}{\hat{u}_{tri}} \qquad\qquad m_f = \frac{f_{sw}}{f_1} \tag{2.10}$$

where $\hat{u}_{ctrl}$ is the control signal used for modulating the duty ratio of the transistors, and f_1 the fundamental frequency of the control signal and the desired output voltage. The voltage $\hat{u}_{tri}$ is the amplitude of the carrier signal whose frequency f_{sw} is also the transistor switching frequency.

The fundamental-frequency phase-to-neutral voltage has, *on average*, an amplitude

$$\hat{u}_s = m_a \frac{U_{dc}}{2} \tag{2.11}$$

providing that the modulator operates in the linear region, i.e. $m_a \leq 1.0$. According to Holtz (1994), the voltage can be increased if third harmonics are added to the control signals u_{ctrl}. For example, if 16.7% of third harmonic is added, Equation (2.11) can be replaced with

$$\hat{u}_s := \frac{2}{\sqrt{3}}\hat{u}_s = m_a \frac{U_{dc}}{\sqrt{3}} \approx 0.577 \cdot m_a U_{dc}. \tag{2.12}$$

Dead-time

In practice, the obtained output voltage is reduced due to the added transistor dead-time (blanking time), during which none of the two transistors in one of the three inverter-legs are conducting to avoid short-circuiting the filter capacitor. Thus, the output voltage floats and is characterized by the magnitude and the direction of the load current i_s and, therefore, on the load's displacement power factor $\cos\varphi_1$ as well.

According to Ruff and Grotstollen (1996), the dead-time is defined as the difference between the switch-on delay time $t_{d,swon}$ of the non-conducting transistor and the turn-off time $t_{off}(i_s)$ of the conducting one

$$t_d(i_s) = t_{d,swon} - t_{off}(i_s). \tag{2.13}$$

If the current rise and fall times, t_r and t_f, and the base drive turn-on and turn-off delays, $t_{d,on}$ and $t_{d,off}$, are taken into account, the definition becomes

$$t_d(i_s) = t_{d,swon} + t_{d,on} - t_{d,off}(i_s) - t_f(i_s). \tag{2.14}$$

Figure 2.3 illustrates the case. The dead-time is chosen conservatively as it is difficult to estimate the current tail time t_{ct} present in some transistor types, for example, in insulated-gate bipolar transistors.

There exists several methods for compensating errors in the output voltage caused by the dead-time varying from the simplest averaging methods to model-reference adaptive control methods. One interesting method is the pulse-based dead-time

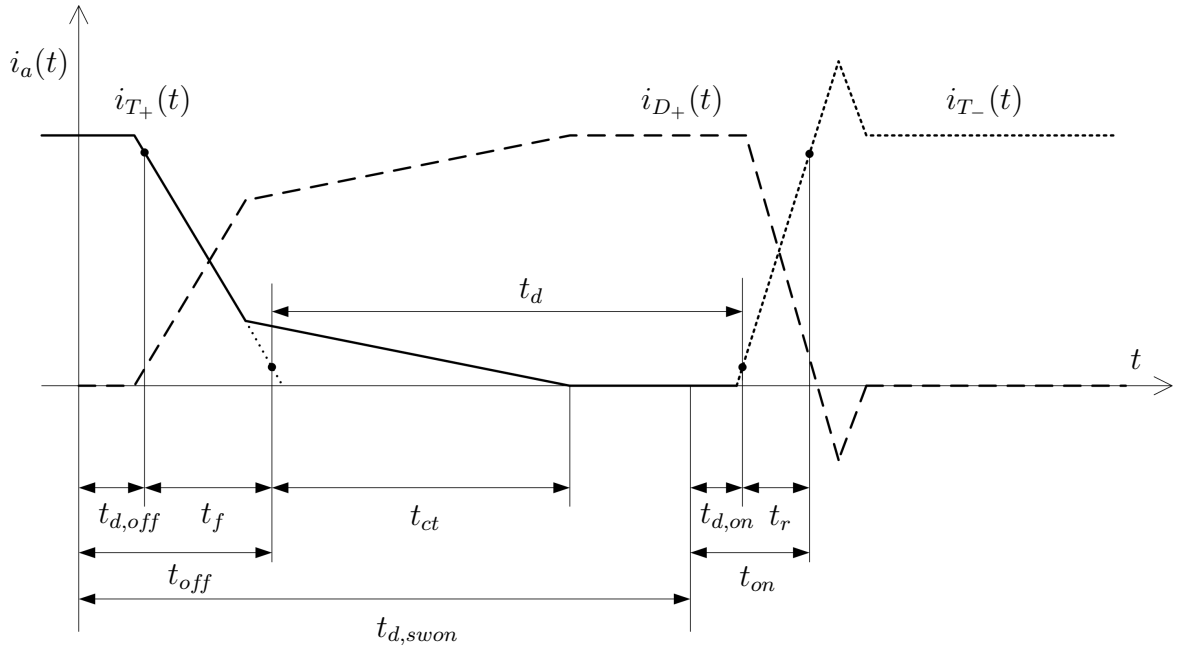

Figure 2.3: Diode-IGBT current switching characteristics for one inverter-leg, according to Martin (1996). T_+ refers to the upper and T_- to the lower transistor and D_+ is the freewheeling diode of the upper transistor.

compensation, which has an ability to reconstruct the magnitude and phase of the output voltage as if the dead-time was not generated at all (Leggate and Kerkman, 1997).

In addition to the nonlinear inverter voltage drop, the output voltage is reduced by the voltage drops over the power transistors, the freewheeling diodes and the motor cabling. Therefore, the output voltage differs from the commanded voltage, which imposes problems in motor identification as the phase voltages are not directly measured. Instead, the output voltages are estimated from the modulation index m_a and the measured DC filter capacitor voltage as in Equation (2.11). The following articles provide a good starting point for a study of methods used for compensating different inverter nonlinearities: (Blaabjerg and Pedersen, 1994), (Choi and Soul, 1994), (Muñoz and Lipo, 1999) and (Urasaki et al., 2005).

Current Measurement

The situation is a bit easier for the motor currents as two of the three phase currents are measured and the third one can be calculated as a linear combination of the first two

$$i_{sa}(t) + i_{sb}(t) + i_{sc}(t) = 0. \tag{2.15}$$

The phase currents are usually filtered in hardware before being measured. Thus, the obtained currents are delayed versions of the real ones as can be observed from

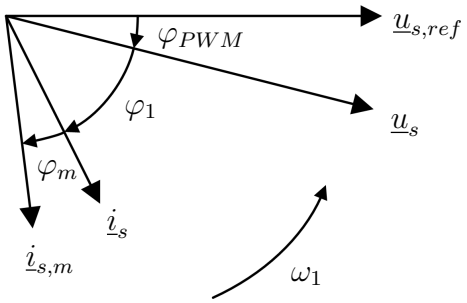

Figure 2.4: Vector diagram of the inverter output voltage and current. $\underline{u}_{s,ref}$ is the commanded voltage and $\underline{i}_{s,m}$ the measured current. The angles φ_{PWM} and φ_m are exaggerated for clarity.

the vector diagram in Figure 2.4.

The magnitude and phase errors caused by the filter can easily be compensated in software. For example, if the output current is filtered with a first-order low-pass filter

$$G_f(\mathrm{j}\omega) = \frac{\omega_0}{\omega_0 + \mathrm{j}\omega} \tag{2.16}$$

where ω_0 is the filter bandwidth, the magnitude and phase of the filter output can be obtained from

$$|G_f(\mathrm{j}\omega)| = \frac{1}{\sqrt{1 + \left(\frac{\omega}{\omega_0}\right)^2}} \tag{2.17a}$$

$$\varphi_m = -\arctan\left(\frac{\omega}{\omega_0}\right). \tag{2.17b}$$

3 Induction Motor Theory

In this chapter, the structure of the induction motor is explained followed by a review of the equations characterizing its electrical and mechanical behavior.

3.1 Structure and Operating Principle

The induction motor consists of a round and hollow static part with a cylindrical rotating part inside of it. The former is referred to as the stator and the latter as the rotor. The stator core has slots inside of its inner surface and the rotor inside of its outer surface. The stator slots of a three-phase motor contain three sets of windings each separated by 120 electrical degrees, whereas the rotor slots contain conducting bars enclosed by short-circuit rings at both ends. A motor with a rotor circuit of this type is called a squirrel-cage induction motor. An alternative configuration is the slip-ring induction motor, whose rotor winding is connected to slip-rings at the motor shaft, from which it is possible to connect the rotor winding to external resistors or to a frequency converter. The stator and rotor cores are made of high-permeability materials to achieve small reluctances in the path of the magnetic fluxes, which is needed to produce maximal magnetic flux with minimal magnetizing current. The mutual inductance between the stator and rotor windings is characterized by the width of the air gap – the smaller the gap, the greater the inductance. On the other hand, the stator and rotor leakage inductances are mainly determined by the shape of the respective windings and slots.

When the stator windings are fed with symmetric sinusoidal voltages whose angular frequency is ω_1, the resulting currents create a rotating magnetic field in the magnetic circuit formed by the stator and rotor cores and the air gap between them. The field rotates at a geometrical angular frequency

$$\Omega_g = \frac{\omega_1}{p} \tag{3.1}$$

where the parameter p is the number of pole pairs formed by the stator windings. This rotating magnetic field induces electromotive forces (emf) in the closed rotor circuit. The currents caused by these emfs produce a magnetic field opposing the rotating stator field. Now, according to Lenz's law, a force will act on a current-carrying conductor placed in a magnetic field. Thus, the rotor bars will be pushed by a tangential magnetic force, producing electrical torque with respect to the rotor shaft. The rotor begins to rotate if the electrical torque is not balanced by an opposite mechanical torque, which further means that the rotor will not rotate exactly at the same, synchronous, angular speed Ω_g as the stator field does. Instead, the rotor will start to rotate asynchronously with a mechanical angular speed

$$\Omega_r = \frac{\omega_r}{p} = \frac{\omega_1 - \omega_2}{p} \tag{3.2}$$

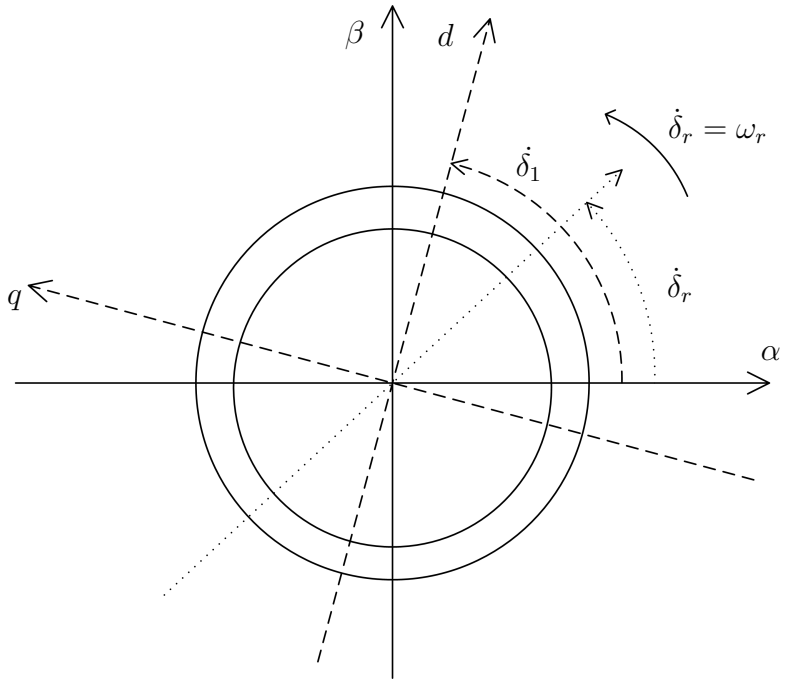

Figure 3.1: Stator and synchronous coordinate axes.

where ω_r is the electrical angular speed of the rotor and ω_2 the angular slip frequency. More detailed explanation of the motor structure and operating principle can be found in (Sadarangani, 2000) and (Krishnan, 2001).

3.2 Electrical Model

The induction motors considered in this thesis have three-phase stator windings. Voltages, currents and flux linkages in such a three-phase system are compactly described by space vectors, which were first proposed in 1959 by Kovács and Rácz according to Holtz (1995). A general space vector is defined as a complex variable

$$\underline{x}^s(t) = x_\alpha(t) + \mathrm{j}x_\beta(t) = \frac{2}{3}\Big[x_a(t) + \mathrm{e}^{\mathrm{j}2\pi/3}x_b(t) + \mathrm{e}^{-\mathrm{j}2\pi/3}x_c(t)\Big] \tag{3.3}$$

where the quantities in the three phases are denoted by the subscripts a, b and c. The space vector maps a three-phase system into a two-phase system with α and β coordinate axes as is illustrated in Figure 3.1. The stator reference frame is fixed to the $\alpha\beta$ axes. The other coordinate system used, in the soon to be introduced model of induction motor, is the synchronous reference frame with d and q coordinate axes. The subscript d stands for direct and q for quadrature. The synchronous reference frame rotates with the angular frequency of the stator current. Transformation between the two coordinate systems is defined as

$$\underline{x}(t) = x_d(t) + \mathrm{j}x_q(t) = \mathrm{e}^{-\mathrm{j}\delta_1}\underline{x}^s(t) \tag{3.4}$$

where the transformation angle δ_1 is defined as

$$\delta_1 = \int \omega_1 \mathrm{d}t. \tag{3.5}$$

The synchronous reference frame is used because all control signals that vary sinusoidally in the stator reference frame became constants. Consequently, such signals can easily be controlled with regular proportional-integral (PI) controllers without steady-state error.

As zero-sequence components cannot be described with space vectors, such components have to be handled separately as the averages in the three phases

$$x_0(t) = \frac{1}{3}\left[x_a(t) + x_b(t) + x_c(t)\right]. \tag{3.6}$$

All variables defined in the stator reference frame are denoted by right superscripts s. For the synchronous reference frame the superscripts are omitted. The superscripts are also omitted if the motor does not rotate, in which case both reference frames are equal.

T Equivalent Circuit

The induction motor resembles a transformer whose secondary winding is free to move; therefore, it has almost same equivalent circuit, Figure 3.2, with only a slight change caused by the rotor-emf $\mathrm{j}\omega_r \underline{\psi}_r^s$. The stator and rotor voltage equations for the induction motor with a squirrel-cage rotor are

$$\frac{\mathrm{d}\underline{\psi}_s^s}{\mathrm{d}t} = \underline{u}_s^s - R_s \underline{i}_s^s \tag{3.7a}$$

$$\frac{\mathrm{d}\underline{\psi}_r^s}{\mathrm{d}t} = \mathrm{j}\omega_r \underline{\psi}_r^s - R_r \underline{i}_r^s \tag{3.7b}$$

where $\underline{\psi}_s^s$ and $\underline{\psi}_r^s$ are the stator and rotor flux linkages, R_s and R_r the stator and rotor resistances, respectively. The flux linkages are defined as

$$\underline{\psi}_s^s = \underline{\psi}_{s\sigma}^s + \underline{\psi}_m^s \tag{3.8a}$$

$$\underline{\psi}_r^s = \underline{\psi}_{r\sigma}^s + \underline{\psi}_m^s \tag{3.8b}$$

$$\underline{\psi}_{s\sigma}^s = L_{s\sigma} \underline{i}_s^s \tag{3.8c}$$

$$\underline{\psi}_{r\sigma}^s = L_{r\sigma} \underline{i}_r^s \tag{3.8d}$$

$$\underline{\psi}_m^s = L_m \underline{i}_m^s \tag{3.8e}$$

where $\underline{\psi}_m^s$, $\underline{\psi}_{s\sigma}^s$ and $\underline{\psi}_{r\sigma}^s$ are the main flux linkage and the stator and rotor leakage flux linkages, respectively. L_m, $L_{s\sigma}$ and $L_{r\sigma}$ are the magnetizing inductance and the stator and rotor leakage inductances, correspondingly. The magnetizing current $\underline{i}_m^s$ is the sum of the stator and rotor currents, $\underline{i}_s^s$ and $\underline{i}_r^s$, if the core loss current $\underline{i}_{Fe}^s$

and resistance R_{Fe} are neglected as they usually are, particularly if the motor is not operated with field-weakening (Levi et al., 1996). All rotor variables are reduced to the stator-side.

For control purposes, it is useful to take the stator current and the rotor flux linkage as the state variables as most frequency converters have a closed-loop current control whose current measurements can be used, and because the rotor flux linkage can be estimated (Holtz, 1995). With this choice, Equations (3.7) become

$$\left(L_s - \frac{L_m^2}{L_r}\right)\frac{\mathrm{d}\underline{i}_s^s}{\mathrm{d}t} = \underline{u}_s^s - \left(R_s + R_r\frac{L_m^2}{L_r^2}\right)\underline{i}_s^s + \left(\frac{R_r}{L_r} - \mathrm{j}\omega_r\right)\frac{L_m}{L_r}\underline{\psi}_r^s \tag{3.9a}$$

$$\frac{\mathrm{d}\underline{\psi}_r^s}{\mathrm{d}t} = R_r\frac{L_m}{L_r}\underline{i}_s^s - \left(\frac{R_r}{L_r} - \mathrm{j}\omega_r\right)\underline{\psi}_r^s \tag{3.9b}$$

where the stator and rotor self-inductances, $L_s = L_m + L_{s\sigma}$ and $L_r = L_m + L_{r\sigma}$, have been used.

Inverse-Γ Equivalent Circuit

In the inverse-Γ model of Figure 3.3, the rotor leakage inductance is transformed to the stator side and combined with the stator leakage inductance to form a total leakage inductance L_σ. This choice reduces the number of parameters by one, and is thus more suitable for control purposes and motor identification as the individual leakage inductances have little effect on motor control.

From Equations (3.9), the transformed rotor variables and parameters can be defined

$$\underline{\psi}_R^s = \frac{L_m}{L_r}\underline{\psi}_r^s \tag{3.10}$$

$$\underline{i}_R^s = \frac{L_r}{L_m}\underline{i}_r^s \tag{3.11}$$

$$\underline{i}_M^s = \underline{i}_s^s + \underline{i}_R^s \tag{3.12}$$

$$L_M = \frac{L_m^2}{L_r} \tag{3.13}$$

$$L_\sigma = L_s - L_M \tag{3.14}$$

$$R_R = \left(\frac{L_m}{L_r}\right)^2 R_r \tag{3.15}$$

where L_M and R_R are the transformed magnetizing inductance and rotor resistance, respectively.

These new definitions change the stator and rotor flux linkages (3.8) to

$$\underline{\psi}_s^s = \underline{\psi}_\sigma^s + \underline{\psi}_R^s \tag{3.16a}$$

$$\underline{\psi}_\sigma^s = L_\sigma\underline{i}_s^s \tag{3.16b}$$

$$\underline{\psi}_R^s = L_M\underline{i}_M^s \tag{3.16c}$$

and the voltage equations (3.7) to

$$\frac{\mathrm{d}\underline{\psi}_s^s}{\mathrm{d}t} = \underline{u}_s^s - R_s\underline{i}_s^s \tag{3.17a}$$

$$\frac{\mathrm{d}\underline{\psi}_R^s}{\mathrm{d}t} = \mathrm{j}\omega_r\underline{\psi}_R^s - R_R\underline{i}_R^s. \tag{3.17b}$$

By substituting Equations (3.10)–(3.16) to the new voltage equations (3.17), the state variable equations (3.9) transform to

$$L_\sigma\frac{\mathrm{d}\underline{i}_s^s}{\mathrm{d}t} = \underline{u}_s^s - (R_s + R_R)\underline{i}_s^s + \left(\frac{R_R}{L_M} - \mathrm{j}\omega_r\right)\underline{\psi}_R^s \tag{3.18a}$$

$$\frac{\mathrm{d}\underline{\psi}_R^s}{\mathrm{d}t} = R_R\underline{i}_s^s - \left(\frac{R_R}{L_M} - \mathrm{j}\omega_r\right)\underline{\psi}_R^s. \tag{3.18b}$$

In synchronous frame, the above equations are

$$L_\sigma\frac{\mathrm{d}\underline{i}_s}{\mathrm{d}t} = \underline{u}_s - (R_s + R_R + \mathrm{j}\omega_1 L_\sigma)\underline{i}_s + \left(\frac{R_R}{L_M} - \mathrm{j}\omega_r\right)\underline{\psi}_R \tag{3.19a}$$

$$\frac{\mathrm{d}\underline{\psi}_R}{\mathrm{d}t} = R_R\underline{i}_s - \left(\frac{R_R}{L_M} + \mathrm{j}\omega_2\right)\underline{\psi}_R. \tag{3.19b}$$

Steady State Inverse-Γ Equivalent Circuit

In steady state, the differential operators in Figure 3.3 can be replaced with $\mathrm{j}\omega_1$ if sinusoidal input voltages and currents are being used. With some algebraic manipulations, Equation (3.17) transforms to

$$\underline{U}_s^s = R_s\underline{I}_s^s + \mathrm{j}\omega_1\left(L_\sigma + L_M\right)\underline{I}_s^s + \mathrm{j}\omega_1 L_M\underline{I}_R^s \tag{3.20a}$$

$$\underline{I}_R^s = -\frac{\mathrm{j}\omega_1 L_M}{\frac{\omega_1}{\omega_2}R_R + \mathrm{j}\omega_1 L_M}\underline{I}_s^s \tag{3.20b}$$

where a symmetric three-phase supply is assumed with 120-degree phase shift between respective voltages and currents. The phasor representation

$$\underline{U}_s^s = U_s\mathrm{e}^{j\omega_1 t} = U_s\angle 0^\circ \tag{3.21a}$$

$$\underline{I}_s^s = I_s\mathrm{e}^{j(\omega_1 t - \varphi_1)} = I_s\angle -\varphi_1 \tag{3.21b}$$

is used for sinusoidal variables. Figure 3.4 shows the corresponding equivalent circuit for the steady state conditions.

Equation (3.20) suggests an expression for the motor impedance

$$\underline{Z}_s^s = R_s + \frac{\omega_1 L_M\omega_2\tau_r}{1 + (\omega_2\tau_r)^2} + \mathrm{j}\omega_1\left[L_\sigma + \frac{L_M}{1 + (\omega_2\tau_r)^2}\right] = R_e + \mathrm{j}\omega_1 L_e \tag{3.22}$$

where τ_r is the rotor time constant L_M/R_R, and R_e and L_e the effective stator resistance and inductance, respectively. From now on, the right superscript s is omitted in complex phasors.

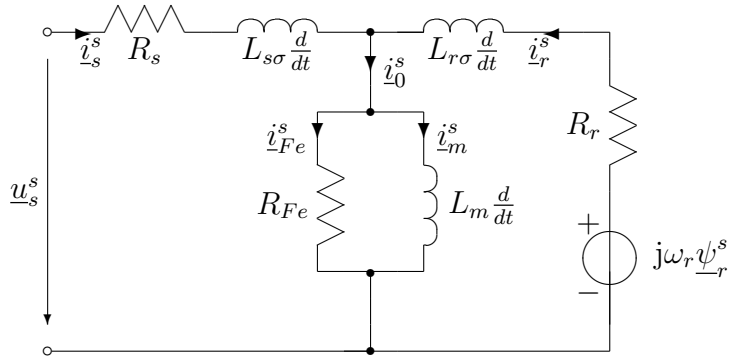

Figure 3.2: Dynamic T equivalent circuit.

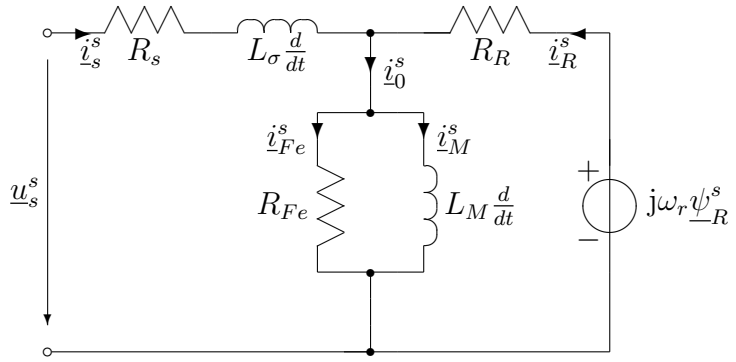

Figure 3.3: Dynamic inverse-Γ equivalent circuit.

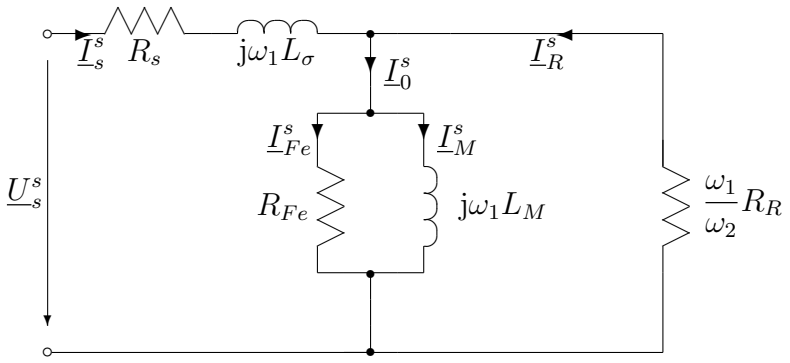

Figure 3.4: Steady state *per-phase* inverse-Γ equivalent circuit.

Electrical Power

The instantaneous apparent three-phase input power $\underline{S}_{in}(t)$ taken from the frequency converter or the supply network is defined as

$$\underline{S}_{in}(t) = \frac{3}{2}\underline{u}_s^s(t)\big(\underline{i}_s^s(t)\big)^* = P_{in}(t) + \mathrm{j}Q_{in}(t) \tag{3.23}$$

and the active and reactive input powers, $P_{in}(t)$ and $Q_{in}(t)$, as

$$P_{in}(t) = u_{sa}(t)i_{sa}(t) + u_{sb}(t)i_{sb}(t) + u_{sc}(t)i_{sc}(t) \tag{3.24a}$$

$$= \frac{3}{2}\Big(u_{s\alpha}(t)i_{s\alpha}(t) + u_{s\beta}(t)i_{s\beta}(t)\Big) \tag{3.24b}$$

$$Q_{in}(t) = \frac{1}{\sqrt{3}}\Big[u_{sa}(t)\Big(i_{sc}(t) - i_{sb}(t)\Big) + u_{sb}(t)\Big(i_{sa}(t) - i_{sc}(t)\Big) + u_{sc}(t)\Big(i_{sb}(t) - i_{sa}(t)\Big)\Big] \tag{3.24c}$$

$$= \frac{3}{2}\Big(u_{s\beta}(t)i_{s\alpha}(t) - u_{s\alpha}(t)i_{s\beta}(t)\Big). \tag{3.24d}$$

In steady state, the three-phase power is constant

$$S_{in} = |\underline{S}_{in}| = \sqrt{P_{in}^2 + Q_{in}^2} = 3U_sI_s = \frac{3}{2}\sqrt{(u_{s\alpha}^2 + u_{s\beta}^2)(i_{s\alpha}^2 + i_{s\beta}^2)} \tag{3.25a}$$

$$P_{in} = 3U_sI_s\cos\varphi_1 = \frac{3}{2}\Big(u_{s\alpha}i_{s\alpha} + u_{s\beta}i_{s\beta}\Big) \tag{3.25b}$$

$$Q_{in} = 3U_sI_s\sin\varphi_1 = \frac{3}{2}\Big(u_{s\beta}i_{s\alpha} - u_{s\alpha}i_{s\beta}\Big) \tag{3.25c}$$

where the parameter φ_1 is the angle between the fundamental-frequency stator voltage and current phasors.

3.3 Mechanical Model

The *motor* mechanics are given by the equation of motion

$$J_e\frac{\mathrm{d}\Omega_r(t)}{\mathrm{d}t} = T_e(t) - T_l(t) \tag{3.26}$$

where the parameter J_e is the system's moment of inertia reduced to the rotor shaft. The variables, T_e, and T_l, are the electrical torque produced by the motor and the torque caused by the load.

The electrical torque is defined as

$$T_e = \frac{3}{2}p\,\mathrm{Im}\left\{(\underline{\psi}_R^s)^*\underline{i}_s^s\right\} = \frac{3}{2}p\,\mathrm{Im}\left\{\underline{\psi}_R^*\underline{i}_s\right\} = \frac{3}{2}p(\psi_{Rd}i_{sq} - \psi_{Rq}i_{sd}), \tag{3.27}$$

which, for the control purposes, is given in the synchronous frame.

4 Motor Control

This chapter describes how the induction motor is controlled as a DC motor in the vector control scheme based on indirect rotor field orientation. The knowledge of this is necessary as it gives the means to understand how the motor behavior is affected by the choice of incorrect controller parameters or by the deviations in the actual motor parameters. Other possible control methods are, e.g., the slip speed compensated U/f-control, which is based on the steady state equations (Stolt, 2005); or the direct torque control (DTC), which is based on the hysteresis control of the stator flux linkage and the electrical torque (Harnefors, 2003).

The modern control system of an induction motor is based on previously introduced complex-valued electrical and mechanical differential equations (3.18) or (3.19) and (3.26). Those equations have to be separated into the real and imaginary parts so that the motor can be controlled with a digital signal processor. The separation reveals a nonlinear and strongly cross-coupled system of equations

$$\begin{aligned} L_\sigma \frac{\mathrm{d}i_{sd}(t)}{\mathrm{d}t} &= u_{sd}(t) - (R_s + R_R) i_{sd}(t) + L_\sigma \omega_1(t) i_{sq}(t) \\ &\quad + \frac{R_R}{L_M} \psi_{Rd}(t) + \omega_r(t) \psi_{Rq}(t) \end{aligned} \tag{4.1a}$$

$$\begin{aligned} L_\sigma \frac{\mathrm{d}i_{sq}(t)}{\mathrm{d}t} &= u_{sq}(t) - (R_s + R_R) i_{sq}(t) - L_\sigma \omega_1(t) i_{sd}(t) \\ &\quad + \frac{R_R}{L_M} \psi_{Rq}(t) - \omega_r(t) \psi_{Rd}(t) \end{aligned} \tag{4.1b}$$

$$\frac{\mathrm{d}\psi_{Rd}(t)}{\mathrm{d}t} = R_R i_{sd}(t) - \frac{R_R}{L_M} \psi_{Rd}(t) + \omega_2(t) \psi_{Rq}(t) \tag{4.1c}$$

$$\frac{\mathrm{d}\psi_{Rq}(t)}{\mathrm{d}t} = R_R i_{sq}(t) - \frac{R_R}{L_M} \psi_{Rq}(t) - \omega_2(t) \psi_{Rd}(t) \tag{4.1d}$$

$$J \frac{\mathrm{d}\omega_r(t)}{\mathrm{d}t} = \frac{3p^2}{2} \psi_{Rd}(t) i_{sq}(t) - \frac{3p^2}{2} \psi_{Rq}(t) i_{sd}(t) - p T_l(t). \tag{4.1e}$$

The couplings between the different complex-valued first-order subsystems can be removed as each system has its own dynamics given by the time constants $\tau_s' = L_\sigma/(R_s + R_R)$, $\tau_r = L_M/R_R$ and $\tau_m = J/b$ for the stator current, rotor flux linkage and mechanical dynamics, respectively. The bandwidths of the subsystem dynamics are separated, stator current dynamics being the fastest and mechanical the slowest, i.e. $\tau_s' \ll \tau_r \ll \tau_m$. Therefore, each control loop can be designed independently. Figure 4.1 illustrates such a cascaded control system.

The couplings between the components of the stator current and the stator angular frequency in Equations 4.1a and 4.1b are easily removed by subtracting the corresponding products from the current controller's output if only the total leakage inductance is known

$$u_{sd}(t) = u_{sd}'(t) - \widehat{L}_\sigma \omega_1(t) i_{sq}(t) \tag{4.2a}$$

$$u_{sq}(t) = u_{sq}'(t) + \widehat{L}_\sigma \omega_1(t) i_{sd}(t) \tag{4.2b}$$

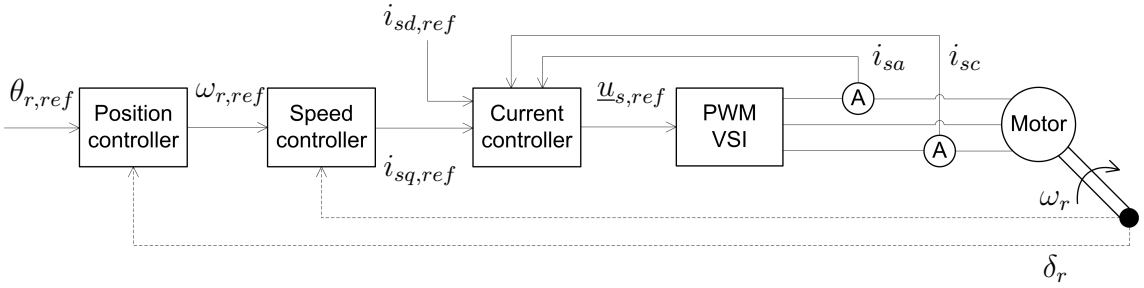

Figure 4.1: Cascaded motor control system.

u'_{sd} and u'_{sq} are the current controller's outputs. This choice reduces the stator current dynamics to

$$L_\sigma \frac{\mathrm{d}i_{sd}(t)}{\mathrm{d}t} = u'_{sd}(t) - (R_s + R_R)i_{sd}(t) + \frac{R_R}{L_M}\psi_{Rd}(t) + \omega_r(t)\psi_{Rq}(t) \tag{4.3a}$$

$$L_\sigma \frac{\mathrm{d}i_{sq}(t)}{\mathrm{d}t} = u'_{sq}(t) - (R_s + R_R)i_{sq}(t) + \frac{R_R}{L_M}\psi_{Rq}(t) - \omega_r(t)\psi_{Rd}(t). \tag{4.3b}$$

But there still exists bilinear nonlinearities between the electrical angular speed of the rotor and the components of the rotor flux linkage. However, these couplings can easily be removed by keeping the rotor flux linkage constant, or the term could be removed completely if the speed were measured, and the value of the magnetizing inductance were known.

4.1 Rotor Field Orientation

The rotor field orientation is the key in controlling the induction motor as a DC motor. This orientation is obtained if the d-axis of the synchronous frame is fixed into the direction of the rotor flux linkage

$$\theta_1 = \arg \underline{\psi}^s_R. \tag{4.4}$$

Thus, the rotor flux linkage becomes real-valued

$$\underline{\psi}_R = \psi_{Rd} + \mathrm{j}\psi_{Rq} = \psi_R. \tag{4.5}$$

Such an orientation transforms the rotor flux linkage equations (4.1c) and (4.1d) into

$$\frac{\mathrm{d}\psi_R(t)}{\mathrm{d}t} = R_R i_{sd}(t) - \frac{R_R}{L_M}\psi_R(t) \tag{4.6a}$$

$$\omega_2(t) = R_R \frac{i_{sq}(t)}{\psi_R(t)} \tag{4.6b}$$

which further reduce to

$$\psi_R = L_M i_{sd} \tag{4.7a}$$

$$\omega_2(t) = \frac{R_R}{\psi_R} i_{sq}(t) \tag{4.7b}$$

when the rotor flux linkage is kept constant. If the stator d-current and the angular slip frequency are controlled as the equations above suggest, the system (4.1a)–(4.1e) is simplified into a linear system resembling a DC-motor

$$L_\sigma \frac{\mathrm{d}i_{sq}(t)}{\mathrm{d}t} = u'_{sq}(t) - (R_s + R_R)i_{sq}(t) - \psi_R \omega_r(t) \tag{4.8a}$$

$$J \frac{\mathrm{d}\omega_r(t)}{\mathrm{d}t} = \frac{3}{2} p^2 \psi_R i_{sq}(t) - pT_l(t). \tag{4.8b}$$

It is observed that with proper rotor field orientation, the torque and speed can simply be controlled with the stator q-voltage. Therefore, the control performance depends on how accurately the magnitude and the direction of rotor flux linkage can be estimated in Equation (4.4), which, on the other hand, depends on how accurately the motor parameters are known.

4.2 Controller Detuning Effects

As was pointed out in the previous section, the drive performance depends on the use of correct model parameters in the current, speed and position controllers. Unfortunately, the motor parameters change heavily during operation as the stator and rotor resistances change with temperature whereas the leakage and magnetizing inductances change with the magnitude and the direction of the stator current, i.e. with the magnetic saturation and hysteresis of the iron core. Furthermore, the rotor parameters change with frequency due to the skin and proximity effects in the rotor bars. Moreover, the iron losses change with the stator frequency.

The total leakage inductance is one of the most important parameters in the induction motor control as it is used to decouple the control system. A wrong value in the current controller causes pulsations in the produced torque when either the reference torque or rotor flux is changed.

On the other hand, the stator resistance is not that important in the RFO control schemes, although, an incorrect value causes steady state error in the current response, and thus in the torque and rotor flux as well. The U/f method, however, is more sensitive to the stator resistance, particularly when operating with low frequency. The exact knowledge of the stator resistance is needed also in RFO schemes if the rotor speed is not measured but estimated. In general, the number and accuracy of parameters required increases when the number of sensors is reduced as more variables need to be estimated.

The most important parameters in the RFO based motor control are the ones used in estimating the direction of the rotor flux. The second most important parameters are the transformed rotor resistance and magnetizing inductance as the produced

torque directly depends on them

$$T_e(t) = \frac{3}{2} p \psi_R i_{sq}(t) \tag{4.9a}$$

$$\psi_R = \frac{R_R}{\omega_2(t)} i_{sq}(t) = L_M i_{sd}. \tag{4.9b}$$

This is particularly true if the drive is torque-controlled, i.e. the speed and position are not controlled, in which case the slip frequency is held constant while the torque and the rotor flux linkage are controlled. As the rotor resistance increases with temperature, the electrical torque and rotor flux increase as well. As a consequence, the magnetic saturation increases and more current is drawn from the supply decreasing drive efficiency. On the other hand, if the torque reference is so high that the resulting current causes magnetic saturation, the rotor flux decreases and the produced torque becomes smaller than the reference. Hence, the torque control becomes nonlinear with detuned operation, and more energy is consumed.

If the motor is speed-controlled, the actual torque matches the load torque in steady state even though the controller parameters were incorrect thanks to the controller's integral action. However, with detuned operation, the rotor flux is set to a wrong value causing the motor to draw more magnetization current than it would be necessary. As a consequence, the maximum available torque is reduced, and the motor runs warmer.

In addition, a speed-controlled motor is always in a detuned state due to the rotor-bar skin effect unless compensated for such effect as the rotor resistance changes every time the reference torque is changed (White and Hinton, 1995). Furthermore, if iron losses are not modeled, there exists slight orientation error all the time, particularly when the motor is run without load at rated speed, or if field weakening is used (Levi et al., 1996). Models that include magnetic saturation are briefly reviewed in (Slemon, 1989).

5 Motor Identification Methods

In this chapter, different methods for identifying the induction motor parameters are introduced. In literature, these methods have been categorized into off-line identification and on-line estimation methods, respectively. Previously, the off-line methods were performed with the locked rotor and no-load tests, but recently the trend has been on identifying the motor at standstill without locking the rotor mechanically. The on-line methods are then used to track the parameters for possible variations.

Without any sophisticated identification methods, basic knowledge of the motor parameters can be obtained from the motor name-plate. It usually contains at least the nominal values of the following electrical and mechanical quantities: voltage, current, frequency, rotor speed, output power and power factor, from which estimates for the rotor time constant, magnetizing inductance and rotor resistance can be calculated.

The inverse-Γ equivalent circuit of the induction motor has four parameters that need to be known with great accuracy if moderately precise vector control or slip compensated scalar control is going to be used for motor control. Parameters needed are the stator resistance R_s, the total leakage inductance L_σ, the transformed magnetizing inductance L_M and the transformed rotor resistance R_R. Furthermore, the iron loss resistance R_{Fe} should be estimated in torque-driven systems to reduce vibrations.

The following section introduces the motor name-plate, after which the problems in measuring the stator resistance with a frequency converter are discussed. Section 5.3 explains the usual locked rotor and no-load tests, and the following section derives the basic equations for the standstill identification. Then, a literature review is presented in Section 5.5, after which the next three sections concentrate on studying the different identification methods. The last section briefly introduces one useful method for finding the motor's magnetizing curve.

5.1 Motor Name-plate

According to IEC (1994), the AC motor name-plate contains some or all of the following information

- Manufacturer's name or mark
- Manufacturer's serial number or identification mark
- Manufacturer's machine code
- Year of production
- Rated mechanical output power P_{outN} [W] (1 horse power = 745,7 W)

- Rated *phase-to-phase* voltage U_N [V] at rated mechanical output power
- Rated stator current I_N [A]
- Rated stator frequency f_{1N} [Hz]
- Rated speed n_N [rpm]
- Rated (displacement) power factor $\cos\varphi_N$
- Number of pole pairs p
- Number of phases
- Winding configuration (Δ or Y)
- Pull-up torque [Nm] i.e. maximum torque at zero speed
- Breakdown torque [Nm] i.e. maximum torque available at rated speed
- Torque at rated speed T_{eN} [Nm]
- Rotor shaft's moment of inertia J_e [kgm^2]
- Degree of protection provided by enclosures (e.g. IP21)
- Duty class (e.g. S1, S2, ...)
- Insulation class (e.g. F)
- Maximum permissible ambient temperature if other than 40°C

From the name-plate values, the following nominal quantities can be calculated

- Apparent three-phase input power

$$S_{inN} = \sqrt{3} U_N I_N \text{ [VA]} \tag{5.1}$$

- Active three-phase input power, see Figure 5.1,

$$P_{inN} = S_{inN} \cos\varphi_N \text{ [W]} \tag{5.2}$$

- Reactive three-phase input power

$$Q_{inN} = \sqrt{(S_{inN})^2 - (P_{inN})^2} \text{ [Var]} \tag{5.3}$$

- Efficiency as a motor at nominal speed

$$\eta_N = \frac{P_{outN}}{P_{inN}} \tag{5.4}$$

- Stator angular frequency

$$\omega_{1N} = 2\pi f_{1N} \text{ [rad/s]} \tag{5.5}$$

- Mechanical angular speed of the rotor

$$\Omega_{rN} = 2\pi n_N \cdot \frac{1 \text{ min}}{60 \text{ s}} \text{ [rad/s]} \tag{5.6}$$

- Number of pole pairs

$$p = \left\lfloor \frac{\omega_{1N}}{\Omega_{rN}} \right\rfloor \tag{5.7}$$

- Electrical angular speed of the rotor

$$\omega_{rN} = p\Omega_{rN} \text{ [rad/s]} \tag{5.8}$$

- Slip frequency

$$\omega_{2N} = \omega_{1N} - \omega_{rN} \text{ [rad/s]} \tag{5.9}$$

- (Relative) slip

$$s_N = \frac{\omega_{2N}}{\omega_{1N}} = \frac{f_{2N}}{f_{1N}} \tag{5.10}$$

- Torque at rated speed

$$T_{eN} = \frac{P_{outN}}{\Omega_{rN}} \text{ [Nm]} \tag{5.11}$$

- Estimate for the nominal rotor flux linkage

$$\widehat{\Psi}_{RN} \approx \frac{U_N}{\sqrt{3}\omega_{1N}} \text{ [Wb]} \tag{5.12}$$

- Estimate for the rotor resistance

$$\widehat{R}_R = \frac{ps_N U_N^2}{\omega_{1N} T_{eN}} \text{ [}\Omega\text{]} \tag{5.13}$$

- Estimate for the rotor time constant

$$\widehat{\tau}_r = \frac{1}{\omega_{1N} s_N \tan\varphi_N} \text{ [s]} \tag{5.14}$$

- Estimate for the nominal magnetizing inductance

$$\widehat{L}_M = \widehat{R}_R \widehat{\tau}_r \text{ [H]} \tag{5.15}$$

- Very rough estimates for the stator resistance and the total leakage inductance

$$\widehat{R}_s \approx \widehat{R}_R \text{ [}\Omega\text{]} \tag{5.16a}$$

$$\widehat{L}_\sigma \approx (0.05 \ldots 0.10) \cdot \widehat{L}_M \text{ [H]} \tag{5.16b}$$

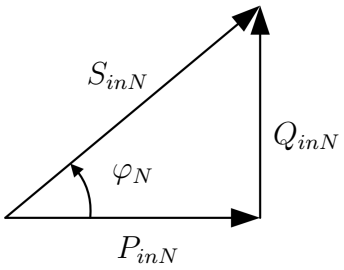

Figure 5.1: Vector diagram of motor power.

5.2 Stator Resistance Measurement

Measuring the DC resistance of a Y connected three-phase stator winding is a very simple task to do with an appropriate bridge ohmmeter as the corresponding value is just a half of the average R_m of the terminal resistances taken between each combination of the stator phases, or three times that if the phases are connected in Δ

$$\widehat{R}_m = \frac{1}{3}\left(\widehat{R}_{ab} + \widehat{R}_{bc} + \widehat{R}_{ca}\right) \tag{5.17a}$$

$$\widehat{R}_{s,\mathrm{Y}} = \frac{\widehat{R}_m}{2} \tag{5.17b}$$

$$\widehat{R}_{s,\Delta} = 3\widehat{R}_{s,\mathrm{Y}} = \frac{3}{2}\widehat{R}_s. \tag{5.17c}$$

However, things are not that simple if the object is to do the measurement with a frequency converter as the inverter voltage drop is a nonlinear function of the stator current due to the generation of the transistor dead-times, and because of the voltage drops caused by the power devices. Figure 5.2 shows the commanded voltage (2.11) of a typical frequency converter as a function of the stator current.

According to Ruff and Grotstollen (1996), the turn-off time of a transistor in one of the inverter legs in Figure 2.2 can be modeled as

$$t_{off}(\underline{i}_s) = t_b + t_a \mathrm{e}^{\kappa|\underline{i}_s|} \tag{5.18}$$

and the corresponding inverter voltage drop as

$$\begin{aligned} |\underline{u}_i(\underline{i}_s)| &= \frac{t_d(\underline{i}_s)}{t_{sw}} U_{dc} = \frac{t_{d,swon} - t_b}{t_{sw}} U_{dc} - \frac{t_a}{t_{sw}} \mathrm{e}^{\kappa|\underline{i}_s|} U_{dc} \\ &= U_{eb} + U_{ea} \mathrm{e}^{\kappa|\underline{i}_s|} \end{aligned} \tag{5.19}$$

where the sum of U_{ea} and U_{eb} is the average of the forward voltage drops over the transistors and the corresponding freewheeling diodes at zero current. The sum is usually near 2.0 volts for the insulated gate bipolar transistors. $t_d(\underline{i}_s)$ is the total dead-time from Equation (2.13) and t_{sw} the switching period. t_b, t_a and κ are the characteristic parameters of the curve.

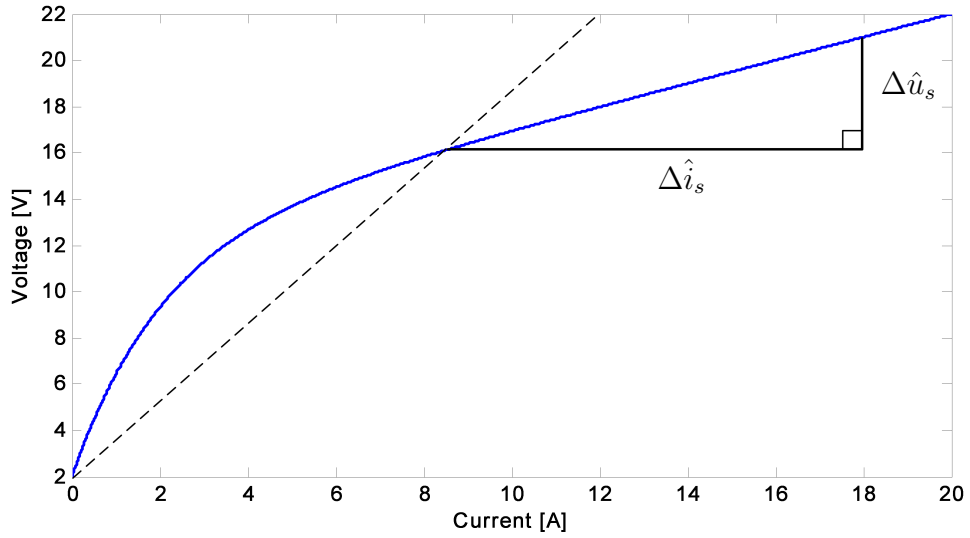

Figure 5.2: The commanded stator voltage as a function of the stator current when the motor is supplied with a frequency converter. The stator resistance is the slope of the linear part.

This nonlinear inverter voltage drop acts as an added resistance $R_i(\underline{i}_s)$ between the current controller's output and the effective stator resistance R_e introduced in Equation (3.22)

$$\underline{u}_{s,ref}(\underline{i}_s) = \underline{u}_i(\underline{i}_s) + \underline{u}_s \tag{5.20a}$$

$$R_{ei}(\underline{i}_s) = R_i(\underline{i}_s) + R_e \tag{5.20b}$$

where the latter equation is obtained from the former by dividing both sides with the stator current space vector, and taking the real part of the result.

It is observed that the stator resistance cannot be separated from the inverter voltage drop without impractical stator phase voltage sensors. However, if the rotor is at standstill and the stator winding is fed with a DC voltage letting the resulting stator current approach infinity, the derivative of Equation (5.20a) with respect to the stator current, i.e. the dynamic resistance $R_D(\underline{i}_s)$, approaches the stator resistance because the coefficient κ is negative in Equation (5.19)

$$R_D(\underline{i}_s) = \frac{\mathrm{d}\underline{u}_{s,ref}(\underline{i}_s)}{\mathrm{d}\underline{i}_s} \tag{5.21a}$$

$$\widehat{R}_s = R_D(\underline{i}_s)\Big|_{\hat{i}_s\to\infty} \approx \frac{\Delta\hat{u}_s}{\Delta\hat{i}_s}. \tag{5.21b}$$

Throughout this thesis, it is assumed that the stator windings of the studied motors are wound with round, small-diameter, conductors, in which case the frequency dependency of the stator resistance, caused by the skin and proximity effects, can be omitted. However, such effects should be modeled if thicker conductors are used.

The above effects caused by the eddy currents are studied in (Hanselman and Peake, 1995).

5.3 Locked Rotor and No-load Tests

This section briefly explains the use of the locked rotor and no-load tests in motor identification. In addition, two equations capable of tracking variations in the iron loss resistance and the transformed magnetizing inductance during operation are introduced.

Locked Rotor Test

The locked rotor test is used to determine the rotor resistance and total leakage inductance. This test is sometimes referred to as a short-circuit test as the motor resembles a transformer whose secondary winding is short-circuited. To perform this test, a three-phase active power meter and both voltage and current meters are needed.

First, the rotor is blocked so it cannot rotate. Then, the machine's stator windings are supplied with sinusoidal voltages U_{sk} causing nominal current flow I_N. The frequency of the sine wave is selected close to the motor's nominal slip frequency f_{2N} as the nominal stator frequency f_{1N} would cause increased rotor resistance due to the skin effect. Furthermore, if a value corresponding to the nominal phase-to-phase voltage U_N were applied, a very high current would flow in the stator windings due to the low stator impedance potentially damaging the rotor-bars. In fact, it is recommended that this test should not last more than 5 seconds at a time and that the motor temperature should not exceed the rated temperature rise plus 40°C, according to (IEEE, 1991, p. 8).

As the rotor is blocked, the parallel magnetizing branch, in the inverse-Γ model of the induction motor, is virtually short-circuited as the slip is unity. The input power is mostly dissipated in the stator and rotor resistances.

From the active power, voltage and current measurements, it is possible to calculate the absolute value for the short-circuit stator impedance and power factor

$$Z_{sk} = \sqrt{R_{sk}^2 + X_{sk}^2} = \frac{U_{sk}}{I_N} \tag{5.22a}$$

$$\cos\varphi_k = \frac{P_{ink}}{S_{ink}} = \frac{P_{ink}}{3U_{sk}I_N} \tag{5.22b}$$

where U_{sk} is the phase-to-neutral voltage, and P_{ink} and S_{ink} the three-phase active and apparent input powers, respectively. These values can be further used to

calculate the short-circuit stator resistance R_{sk} and reactance X_{sk}

$$R_{sk} = \frac{P_k}{3I_N^2} = Z_{sk}\cos\varphi_k = R_s + R_R \tag{5.23a}$$

$$X_{sk} = \sqrt{Z_{sk}^2 - R_{sk}^2} = Z_{sk}\sin\varphi_k = X_\sigma \approx X_{s\sigma} + X_{r\sigma} \tag{5.23b}$$

where $X_{s\sigma}$ and $X_{r\sigma}$ are the stator and rotor leakage reactances. Finally, the rotor resistance and total leakage inductance are obtained

$$\widehat{R}_R = R_{sk} - \widehat{R}_s \tag{5.24a}$$

$$\widehat{L}_\sigma = \frac{X_{sk}}{\omega_{2N}} = \frac{X_{sk}}{2\pi f_{2N}}. \tag{5.24b}$$

No-load Test

The no-load test is used to determine the motor's iron loss resistance R_{Fe} and the transformed magnetizing inductance L_M, which are in parallel in the inverse-Γ equivalent circuit

$$\underline{Z}_M = \frac{\underline{U}_M}{\underline{I}_0} = \frac{\mathrm{j}R_{Fe}X_M}{R_{Fe} + \mathrm{j}X_M} \tag{5.25a}$$

$$\underline{U}_M = \underline{U}_{s0} - (R_s + \mathrm{j}X_\sigma)\underline{I}_{s0} \tag{5.25b}$$

where $\underline{U}_M$ and $\underline{I}_0$ are the voltage over and the current in the magnetizing branch, and $\underline{U}_{s0}$ and $\underline{I}_{s0}$ the stator no-load voltage and current, respectively. In some books, e.g. in (Vas, 1993), the effect of the stator resistance is omitted being lower than that of the total leakage reactance

$$U_M \approx U_{s0} - X_\sigma I_{s0}. \tag{5.26}$$

The magnetizing branch is identified by first removing the load from the rotor shaft and then feeding the stator windings with sinusoidal voltages having nominal frequency f_{1N}. The voltage U_{s0} is raised from zero to the value corresponding the nominal phase voltage $U_N/\sqrt{3}$, after which the voltage, current and the active three-phase input power are measured.

The active no-load input power P_{in0} is divided into the mechanical output power P_{out} and to the part heating the motor. The latter consists of several parts, two of which are the resistive losses produced in the stator windings and in the rotor cage, P_{Cus} and P_{Cur}, respectively. Other parts include the iron losses of the stator and

Table 5.1: Assumed Values for Stray-Load Loss (IEEE, 1991, p. 17).

Machine Rating	Stray-Load Loss Percent of Rated Output
1-125 hp	1.8%
126-500 hp	1.5%
501-2499 hp	1.2%
2500 hp and greater	0.9%

rotor cores, P_{Fes} and P_{Fer}, and the losses caused by friction P_{fr} and windage P_{wi}

$$\begin{aligned} P_{in0} &= P_{Cus} + P_{Fes} + P_{Cur} + P_{Fer} + P_{fr} + P_{wi} + P_{out} \\ &= 3U_{s0}I_{s0}\cos\varphi_0 \end{aligned} \tag{5.27a}$$

$$P_{Cus} = 3I_{s0}^2 R_s \tag{5.27b}$$

$$P_{Cur} = 3I_{R0}^2 R_R \tag{5.27c}$$

$$P_{Fes} = 3\frac{U_M^2}{R_{Fe}}. \tag{5.27d}$$

In the above equation, $\cos\varphi_0$ is the no-load power factor similar to the one in (5.22b). The rotor iron losses are usually either included in the stator iron losses or totally omitted as those losses are rather difficult to measure.

In addition to the introduced power losses, there exist losses which do not belong to any of the above groups. These losses are called stray losses P_{str}, and they can be measured correctly only by removing the rotor and subtracting the known losses from the input power. Otherwise, the stray losses have to be estimated from the known power losses with a rather difficult procedure described in (IEEE, 1991, p. 14). However, if the motor complies with the applicable IEC standards, the stray losses can be approximated with the values given in Table 5.1.

The reactive three-phase input power Q_{in0} consists of the reactive powers Q_σ and Q_M consumed in the total leakage inductance and the transformed magnetizing inductance

$$Q_{in0} = Q_\sigma + Q_M = 3U_{s0}I_{s0}\sin\varphi_0 \tag{5.28a}$$

$$= \sqrt{S_{in0}^2 - P_{in0}^2} = \sqrt{(3U_{s0}I_{s0})^2 - P_{in0}^2} \tag{5.28b}$$

$$Q_\sigma = 3I_{s0}^2 X_\sigma = 3I_{s0}^2 \omega_{1N} L_\sigma \tag{5.28c}$$

$$Q_M = 3\frac{U_M^2}{X_M} = 3\frac{U_M^2}{\omega_{1N} L_M}. \tag{5.28d}$$

As there is no load, the rotor will rotate near the synchronous speed ω_{1N}, i.e. the slip is almost zero ($s \approx 0$). Thus, the induced rotor currents are small and the corresponding resistive losses can be neglected.

From the active power, voltage and current measurements, and from Equations (5.25)–(5.28), the iron loss resistance and the transformed magnetizing inductance are obtained

$$\widehat{R}_{Fe} = \quad 3\frac{U_M^2}{P_{Fes}} \quad = 3\frac{U_{s0}^2 + \left[\widehat{R}_s^2 + (\omega_{1N}\widehat{L}_\sigma)^2\right] I_{s0}^2 - \frac{2}{3}(P_{in0}\widehat{R}_s + Q_{in0}\omega_{1N}\widehat{L}_\sigma)}{P_{in0} - 3I_{s0}^2\widehat{R}_s - \widehat{P}_{out}} \tag{5.29a}$$

$$\widehat{L}_M = 3\frac{U_M^2}{\omega_{1N}Q_M} = 3\frac{U_{s0}^2 + \left[\widehat{R}_s^2 + (\omega_{1N}\widehat{L}_\sigma)^2\right] I_{s0}^2 - \frac{2}{3}(P_{in0}\widehat{R}_s + Q_{in0}\omega_{1N}\widehat{L}_\sigma)}{\omega_{1N}(Q_{in0} - 3I_{s0}^2\omega_{1N}\hat{L}_\sigma)}. \tag{5.29b}$$

If the effect of the iron loss resistance is omitted, the magnetizing inductance can also be approximated as

$$\widehat{L}_M = \frac{U_{s0}}{\omega_{1N}I_{s0}} - \widehat{L}_\sigma \approx \frac{U_{s0}}{2\pi f_{1N}I_{s0}}. \tag{5.30}$$

If more precise results were wanted, the rotor should be connected to, e.g., a DC-motor, as it is suggested in (Krishnan, 2001), and rotated at exact synchronous speed to avoid errors caused by slip and the estimation of the mechanical losses in Equation (5.29a).

5.4 Standstill Identification

In this section, the basic equations and conditions for standstill identification are derived.

For identification purposes, the motor equations should contain only directly measurable variables such as the stator voltage and current. This is achieved by substituting the flux linkage equations (3.8) to the stator voltage equations (3.7)

$$L_s\frac{\mathrm{d}\underline{i}_s^s(t)}{\mathrm{d}t} = \underline{u}_s^s(t) - R_s\underline{i}_s^s(t) - L_m\frac{\mathrm{d}\underline{i}_r^s(t)}{\mathrm{d}t} \tag{5.31a}$$

$$L_r\frac{\mathrm{d}\underline{i}_r^s(t)}{\mathrm{d}t} = \mathrm{j}\omega_r L_m\underline{i}_s^s(t) + (\mathrm{j}\omega_r L_r - R_r)\,\underline{i}_r^s(t) - L_m\frac{\mathrm{d}\underline{i}_s^s(t)}{\mathrm{d}t}. \tag{5.31b}$$

To avoid solving a complex-valued system, the above equations are extracted to real and imaginary parts

$$L_s\frac{\mathrm{d}i_{s\alpha}(t)}{\mathrm{d}t} = u_{s\alpha}(t) - R_s i_{s\alpha}(t) - L_m\frac{\mathrm{d}i_{r\alpha}(t)}{\mathrm{d}t} \tag{5.32a}$$

$$L_r\frac{\mathrm{d}i_{r\alpha}(t)}{\mathrm{d}t} = -\omega_r L_m i_{s\beta}(t) - R_r i_{r\alpha}(t) - \omega_r L_r i_{r\beta}(t) - L_m\frac{\mathrm{d}i_{s\alpha}(t)}{\mathrm{d}t} \tag{5.32b}$$

$$L_s\frac{\mathrm{d}i_{s\beta}(t)}{\mathrm{d}t} = u_{s\beta}(t) - R_s i_{s\beta}(t) - L_m\frac{\mathrm{d}i_{r\beta}(t)}{\mathrm{d}t} \tag{5.32c}$$

$$L_r\frac{\mathrm{d}i_{r\beta}(t)}{\mathrm{d}t} = \omega_r L_m i_{s\alpha}(t) + \omega_r L_r i_{r\alpha}(t) - R_r i_{r\beta}(t) - L_m\frac{\mathrm{d}i_{s\beta}(t)}{\mathrm{d}t}. \tag{5.32d}$$

The next step is to Laplace transform Equations (5.32) considering the initial values zero, after which those equations are solved for the components of the stator current

$$\begin{bmatrix} I_{s\alpha}(s) \\ I_{s\beta}(s) \end{bmatrix} = \frac{1}{R_s} \begin{bmatrix} G_1(s) & G_2(s) \\ -G_2(s) & G_1(s) \end{bmatrix} \begin{bmatrix} U_{s\alpha}(s) \\ U_{s\beta}(s) \end{bmatrix}. \tag{5.33}$$

The transfer functions $G_1(s)$ and $G_2(s)$ are defined as

$$G_1(s) = \frac{[\sigma\tau_r\tau_s s^2 + (\tau_r + \tau_s)s + 1](\tau_r s + 1) + (\omega_r\tau_r)^2(\sigma\tau_s s + 1)}{[\sigma\tau_r\tau_s s^2 + (\tau_r + \tau_s)s + 1]^2 + (\omega_r\tau_r)^2(\sigma\tau_s s + 1)^2} \tag{5.34a}$$

$$G_2(s) = \frac{\omega_r\tau_r\tau_s(1-\sigma)s}{[\sigma\tau_r\tau_s s^2 + (\tau_r + \tau_s)s + 1]^2 + (\omega_r\tau_r)^2(\sigma\tau_s s + 1)^2}. \tag{5.34b}$$

The parameters τ_s, τ_r and σ are the stator and rotor time constants and the leakage factor defined as

$$\tau_s = \frac{L_s}{R_s} = \frac{L_\sigma + L_M}{R_s} \tag{5.35}$$

$$\tau_r = \frac{L_r}{R_r} = \frac{L_M}{R_R} \tag{5.36}$$

$$\sigma = 1 - \frac{L_m^2}{L_s L_r} = \frac{L_\sigma}{L_\sigma + L_M}. \tag{5.37}$$

When the motor is at standstill, $\omega_r = 0$, the transfer function $G_2(s)$ is zero and the system dynamics are reduced to

$$I_{s\alpha}(s) = \frac{\tau_r s + 1}{\sigma\tau_r\tau_s s^2 + (\tau_r + \tau_s)s + 1} \cdot \frac{U_{s\alpha}(s)}{R_s} \tag{5.38a}$$

$$I_{s\beta}(s) = \frac{\tau_r s + 1}{\sigma\tau_r\tau_s s^2 + (\tau_r + \tau_s)s + 1} \cdot \frac{U_{s\beta}(s)}{R_s} \tag{5.38b}$$

from which it is observed that the motor parameters can be identified using either α- or β-components. Furthemore, the stator and rotor reference frames become equal. As a consequence, from now on the superscript s is omitted in the space vector notation for convenience.

For real frequencies, the Laplace variable s in the transfer function (5.38) can be replaced by $\mathrm{j}\omega$. Then, a Bode diagram can be plotted for a particular motor by varying the frequency of the input voltage and measuring the magnitude and phase difference of the ratio of the current and voltage. The obtained frequency response looks like the one in Figure 5.3, from which it can be observed that the motor resembles a low-pass filter.

For standstill identification, there are two choices of excitation: **Case 1**, one of the three phases is disconnected, $i_{sb}(t) = 0$, or **Case 2**, two phases are connected together, $i_{sb}(t) = i_{sc}(t)$. Figure 5.4 shows both cases.

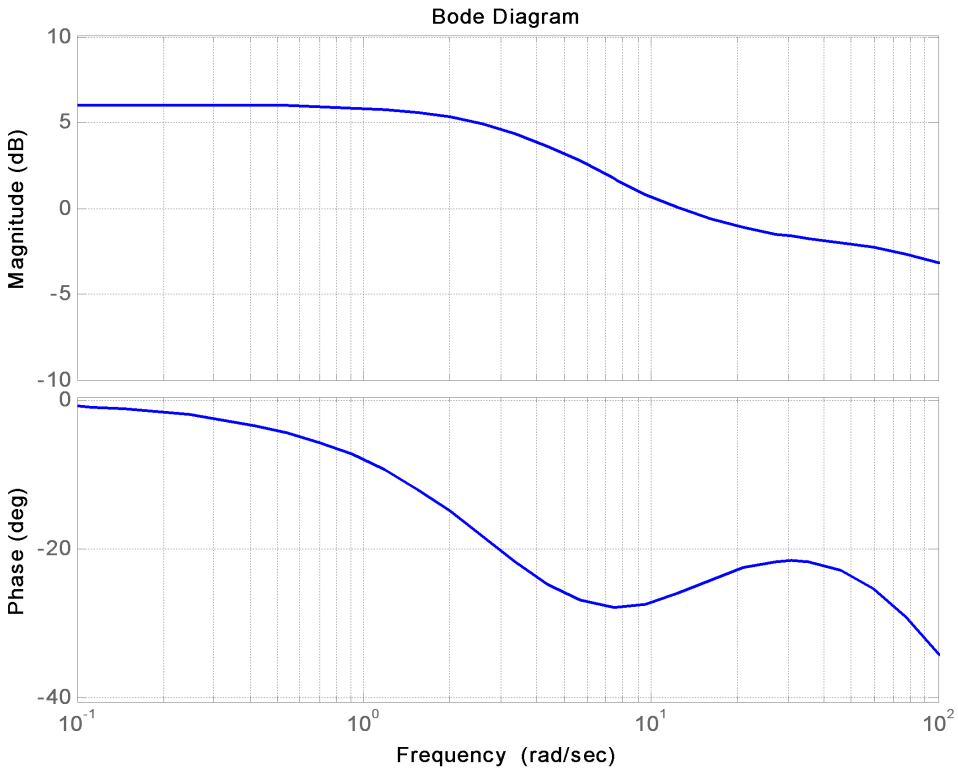

Figure 5.3: Simulated standstill frequency response of an ideal test motor with parameters: $R_s = 0.5\ \Omega$, $R_R = 0.7\ \Omega$, $L_\sigma = 7.3$ mH, $L_M = 65.0$ mH.

For the **Case 1**, the phase b is disconnected, i.e. the current in that phase is zero,

$$0 = i_{sa}(t) + i_{sb}(t) + i_{sc}(t) \tag{5.39a}$$
$$i_{sb}(t) = 0 \tag{5.39b}$$
$$\rightarrow i_{sc}(t) = -i_{sa}(t) \tag{5.39c}$$

and the current space vector becomes

$$\begin{aligned}\underline{i}_s(t) &= \frac{2}{3}\left[i_{sa}(t) - \frac{1}{2}\Big(i_{sb}(t) + i_{sc}(t)\Big) + \mathrm{j}\frac{\sqrt{3}}{2}\Big(i_{sb}(t) - i_{sc}(t)\Big)\right] \\ &= i_{sa}(t) + \mathrm{j}\frac{1}{\sqrt{3}}i_{sa}(t) = \frac{2}{\sqrt{3}}i_{sa}(t)\angle 30°.\end{aligned} \tag{5.40}$$

For the **Case 2**, the phases b and c are connected in parallel, i.e. the same current flows in both phases,

$$0 = i_{sa}(t) + i_{sb}(t) + i_{sc}(t) = i_{sa}(t) + 2i_{sc}(t) \tag{5.41a}$$
$$\rightarrow i_{sc}(t) = i_{sb}(t) = -\frac{1}{2}i_{sa}(t) \tag{5.41b}$$

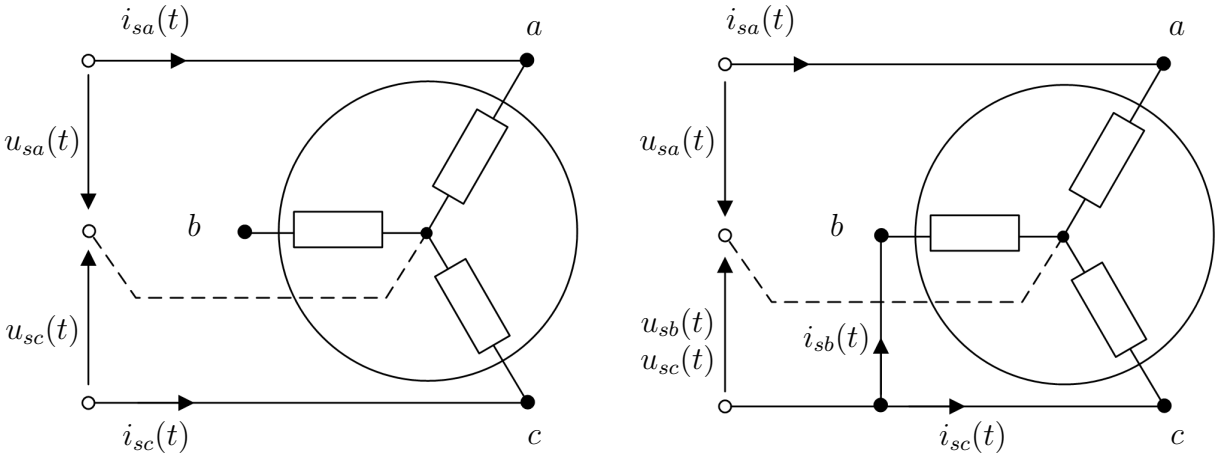

Figure 5.4: The configuration of the stator windings in standstill identification. **Cases 1** and **2** are on the left and right, respectively. Although the connections are made physically in the picture, the same can be done virtually with the inverter.

and the current space vector becomes

$$\begin{aligned}\underline{i}_s(t) &= \frac{2}{3}\left[i_{sa}(t) - \frac{1}{2}\Big(i_{sb}(t) + i_{sc}(t)\Big) + \mathrm{j}\frac{\sqrt{3}}{2}\Big(i_{sb}(t) - i_{sc}(t)\Big)\right] \\ &= \frac{2}{3}\Big(i_{sa}(t) - i_{sc}(t)\Big) = i_{sa}(t). \end{aligned} \tag{5.42}$$

As a consequence, the stator current space vector cannot rotate nor can the rotor. Therefore, the identification can be performed at standstill even without locking the rotor mechanically as no torque is produced (Barrero et al., 1999). Figure 5.5 shows the simulated current waveforms in the **Cases 1** and **2**, respectively.

From Figure 5.4, it can be observed that it is possible to use 33% higher test voltage in **Case 1** than in **Case 2** as the stator impedances are in series instead of being in series/parellel. This is beneficial as the motor is usually fed with voltage-sensorless pulse-width modulated inverter where the motor phase voltage 'measurement' is based on the applied reference voltage, modulation index and dead-time compensation as was seen in Section 2.2.

However, the identified magnetizing inductance is slightly higher with this type of zero-torque excitation compared to the torque-producing three-phase case when the same level of stator flux linkage is used. This phenomenon, which is more pronounced as the magnetic circuit saturates, is caused by the fact that the α- and β-components of the stator flux linkage use partly common iron paths. According to Klaes (1993), the identified values for the magnetizing inductance should be approximately 11% higher with this type of excitation compared to the regular three-phase case. Although an interesting point, for some reason, it has not been discussed further in the reviewed literature.

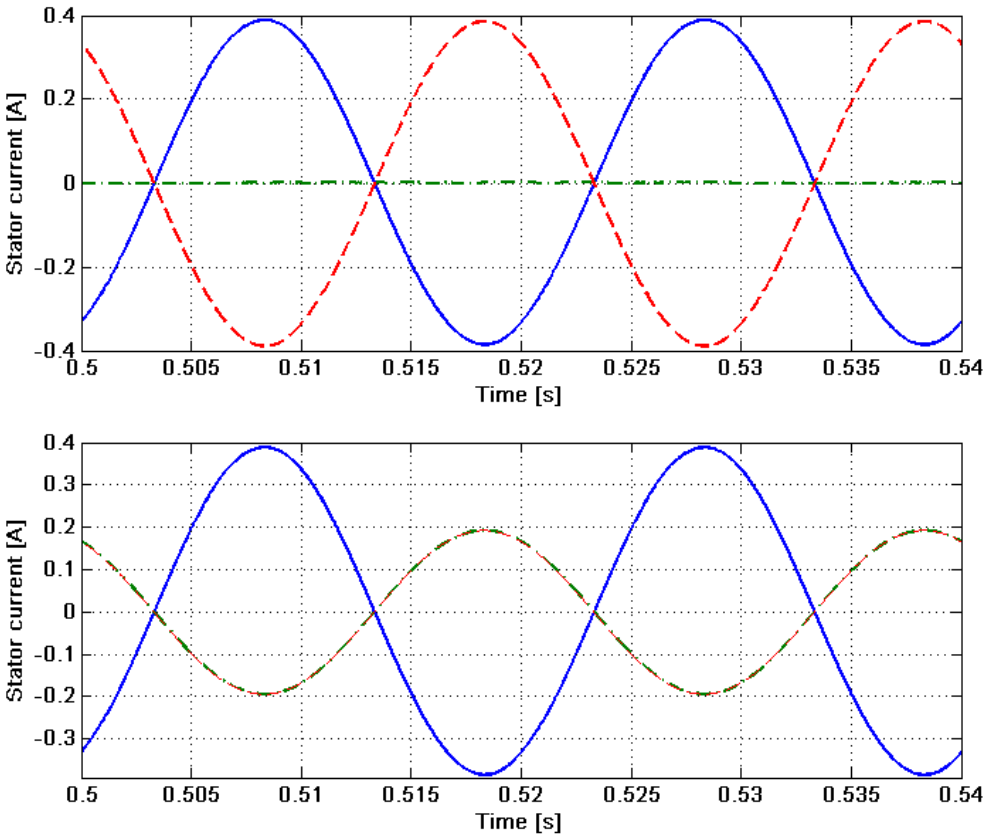

Figure 5.5: Simulated waveforms of sinusoidal stator currents in **Cases 1** (top) and **2** (bottom). Phases a, b and c are drawn with blue, green and red color, respectively.

5.5 Literature Review on Standstill Identification Methods

System identification methods are divided into to time (TD) and frequency domain (FD) methods (Johansson, 1993). When such methods are applied to motor identification, the motor's stator windings are fed with either voltage or current pulses in the former, and with sinusoidal waveforms of selected amplitudes and frequencies in the latter.

The TD approaches are based on the motor's differential equations (3.7) and the FDs on the steady-state equations (3.20). Both methods are susceptible to nonlinearities as the motor models, usually, omit inverter nonlinearities, rotor-bar skin effects, and both saturation and hysteresis effects in the main flux linkage, and when such effects are included, the models become very complex (Bünte and Grotstollen, 1993), (Ruff and Grotstollen, 1996).

In motor identification, the first thing to do is to find correct parameters for the stator windings so that the current controller can be set properly. There are numerous ways to accomplish this task. For instance, Rasmussen et al. (1996) have used an experimental tuning approach based on the well-known Ziegler-Nichols ultimate gain method described in several basic control theory books, for example in (Hägglund and Åström, 2006). After the current controller has been set, if wanted, the motor parameters can be solved from the controller parameters. Others have calculated controller parameters after first identifying the stator parameters.

Problems are caused by the nonlinear inverter voltage drop as it tend to increase the resistance seen by the current controller. Most authors have used sufficiently high input voltages and currents to avoid operating in the nonlinear region in Figure 5.2, which is straightforward when using TD methods. In FD methods, the same effect is achieved when the motor is fed with DC, in addition to the AC. This type of excitation is used, e.g., in (Bertoluzzo et al., 1997), (Seok et al., 1997), (Kwon et al., 2008).

The biggest problem in standstill motor identification is finding the correct value for the constantly varying rotor time constant. During the 1980s, many methods appeared in literature. One common method was to feed the stator with a sinusoidal current with the exact slip frequency, and to switch the stator current to the assumed DC magnetizing current. If the slip frequency and the DC current were correct, no transient could be observed in the stator voltage, and thus the correct rotor time constant had been found for that particular magnetizing current (Wang et al., 1988).

The most common standstill TD methods are based on calculating the stator and rotor time constants from the measured stator currents when the stator is supplied with a DC voltage which is then switched either on or off as is done in (Ambrožić et al., 1993), (Kwon et al., 1994), (Couto and de Aguiar, 1998). The simpler methods rely only on few measurements whereas the more sophisticated ones are based on several measurements, which are fitted to the motor model by, for example, either recursive least squares or maximum likelihood algorithms (Moon and Keyhani, 1993), (Barrero et al., 1999). This way the effect of wrong measurements and noise

can be reduced in the parameter estimates.

The newest methods are based on arbitrary input signals with inverter nonlinearities taken into account as in (Michalik, 1998), where optimal, pseudo-random binary sequence signals have been used, or as in (Aiello et al., 2002), (Cirrincione et al., 2002), (do Prado Junior et al., 2002). Many newer methods are based on solving the motor parameters recursively from discretized motor models. Thus, the identified parameters are affected by the chosen discretization method, the quality of the anti-aliasing filters and the used sampling frequency. Furthermore, the discretized model parameters are mapped to the real, continuous, parameters in a very nonlinear way.

In addition, the recursive curve fitting methods have trouble on converging to the correct values if the input signals are not 'persistently exciting' the system, i.e. signals remain constant for too long periods, as is pointed out by Ljung and Söderström (1983) and Franklin et al. (1990). Such identifiability problems are avoided in continuous-time identification methods reviewed in (Garnier et al., 2003) and (Garnier and Young, 2004). These methods have been developed as early as in the 1950s, according to Johansson (1986), but not used in standstill motor identification before 1985 (Minami et al., 1991). A decade ago, this method has been studied for real-time parameter identification by Dell'Aquila et al. (1994). The continuous-time identification methods are superior compared to the discrete-time methods as the parameter estimates are not dependent on the chosen sampling frequency, and there is no need to use anti-aliasing filters as is mentioned in (Johansson, 1993, p. 308).

The motor flux level is governed by the magnetizing current and the magnetizing inductance. It has been shown by several authors that a constant value for the magnetizing inductance is inadequate alone, and that there is a need to identify both the static and dynamic magnetizing inductances if the motor is going to be operated above the nominal speed with reduced flux, or if the motor's magnetic circuit is very nonlinear. Thus, many have tried to approximate the magnetizing current and flux with different types of analytic functions. For example, Melkebeek and Novotny (1983) have tried the simplest approach by approximating the magnetizing inductance with two straight lines, Kerkman (1985) and Bertoluzzo et al. (2001) have tried 3rd-, 5th- and 7th-order polynomials with seemingly good results whereas Ruff and Grotstollen (1996) have used exponential functions. According to Ganji et al. (1996), transcendental functions, i.e. $\arctan(x)$, $\tanh(x)\ldots$, have also been tried, but such functions should be avoided as those cannot be implemented easily in digital signal processors. In general, the used functions should be continuous, smooth and easily differentiable. As finding the magnetizing curve adds much more complexity to the motor identification, it has often been omitted in industrial applications. Instead of that, a simple table of fixed values with linear interpolation has been used (Niiranen, 1999).

The amount of scientific articles on the motor identification is so vast at the moment, easily more than 200, that the major problem in choosing the right methods has been on finding the simplest ones as most of the studied papers are either too complex for industrial applications or they are concerning parameter estimation in

normal operation conditions with extended Kalman filters, model-reference adaptive system (MRAS) methods, neural networks or other very difficult methods that are not suitable for standstill identification. More on these and many other advanced methods can be found in (Krishnan and Bharadwaj, 1991) and in a very thorough literature review written by Toliyat et al. (2003).

According to the author's opinion, the most suitable standstill identification schemes encountered while reviewing the literature were written by Sukhapap and Sangwongwanich (2002) and Kwon et al. (2008). Those articles effectively summarize the simplest methods used in the time and frequency domains. Furthermore, methods with discrete-time motor models should be avoided.

In the forthcoming sections, the simplest time domain identification method based on a voltage step response is reviewed in Section 5.6. The following Section 5.7 introduces a continuous-time method called state variable filtering capable of identifying any linear time-invariant system. The method is then applied to the induction motor's electrical parameters. Section 5.8 reviews the simplest standstill identification scheme based on frequency response, and Section 5.9 describes one way to identify the magnetizing curve as a function of the magnetizing current.

5.6 Step Response Identification

In this section, it is shown how the motor parameters can be identified in time domain. The idea is to excite the motor with a voltage step and to measure the resulting current response. The measured data is then compared with the data obtained from the corresponding model, from which the desired parameters can be obtained with linear regression.

The mathematical model of the motor whose rotor is at standstill, i.e. the transfer function from the stator voltage to the stator current (5.38a), was already derived in Section 5.4. Here, the model needs only to be excited with a Laplace transformed voltage step $\frac{u_{s\alpha}}{s}$

$$I_{s\alpha}(s) = \frac{u_{s\alpha}}{R_s} \cdot \frac{\tau_r s + 1}{s\left[\sigma\tau_r\tau_s s^2 + (\tau_r + \tau_s)s + 1\right]} \tag{5.43}$$

after which the desired current response is obtained when the transfer function is transformed back into the time domain

$$i_{s\alpha}(t) = \frac{u_{s\alpha}}{R_s}\left\{1 + \frac{1}{2\xi}\left[(\tau_s - \tau_r - \xi)\,\mathrm{e}^{-\frac{\tau_r+\tau_s+\xi}{2\sigma\tau_r\tau_s}t} - (\tau_s - \tau_r + \xi)\,\mathrm{e}^{-\frac{\tau_r+\tau_s-\xi}{2\sigma\tau_r\tau_s}t}\right]\right\}. \tag{5.44}$$

The parameter ξ is used to simplify notation

$$\xi = (\tau_r + \tau_s)\sqrt{1 - \frac{4\sigma\tau_r\tau_s}{(\tau_r + \tau_s)^2}}. \tag{5.45}$$

The total leakage inductance is the easiest parameter to obtain as it can be solved from the tangent of the current response (5.44) evaluated at origin

$$\left.\frac{\mathrm{d}i_{s\alpha}(t)}{\mathrm{d}t}\right|_{t=0} = \frac{u_{s\alpha}}{L_\sigma}$$
$$\rightarrow \widehat{L}_\sigma \approx \frac{\Delta t}{\Delta i_{s\alpha}} u_{s\alpha}. \tag{5.46}$$

The complicated equation of the stator current has to be simplified so that the transformed magnetizing inductance and rotor resistance can be solved. Ambrožić et al. (1993) suggest that the stator current could be approximated with a simpler form

$$i_{s\alpha}(t) \approx \frac{u_{s\alpha}}{R_s}\left(1 - \frac{\tau_s}{\tau_r + \tau_s}\mathrm{e}^{-\frac{t}{\tau_r+\tau_s}}\right) \tag{5.47}$$

where the square root in ξ is replaced with the two first terms in the corresponding Taylor series, and that the leakage factor is omitted. This approximation converges if the term under the square root of ξ fulfills the inequality

$$1 \geq \left|\frac{4\sigma\tau_r\tau_s}{(\tau_r+\tau_s)^2}\right| \approx \sigma > 0, \qquad \text{i.e. if } \tau_r \approx \tau_s. \tag{5.48}$$

According to Ambrožić et al. (1993), the expectable error is then in the range of 3% to 5% for motors with $(0.09 \leq \sigma \leq 0.15)$. In Figure 5.6, the simulated and approximated stator current responses are plotted.

Now, the rotor parameters can be solved from a linear system of equations, which is obtained by taking at least two measurement points from the stator voltage and current at different instants of time, t_1 and t_2. For this purpose, Equation (5.47) has to be transformed into a pseudo-linear form by rearranging it and taking natural logarithms on both sides

$$\ln\left|1 - \frac{R_s}{u_{s\alpha}} i_{s\alpha}(t)\right| = \ln\left|\frac{\tau_s}{\tau_r+\tau_s}\right| - \frac{t}{\tau_r+\tau_s}. \tag{5.49}$$

The above first-order equation represents a straight line in space

$$y(t) = \theta_0 + \theta_1 t = \begin{bmatrix}1 & t\end{bmatrix}\begin{bmatrix}\theta_0 \\ \theta_1\end{bmatrix} = \boldsymbol{\varphi}^T\boldsymbol{\theta} \tag{5.50}$$

where the function $y(t)$ and the parameters θ_0 and θ_1 are defined as

$$y(t) = \ln\left|1 - \frac{R_s}{u_{s\alpha}} i_{s\alpha}(t)\right| \tag{5.51a}$$
$$\theta_0 = \ln\frac{\tau_s}{\tau_r+\tau_s} = \ln\frac{(L_\sigma+L_M)R_R}{(L_\sigma+L_M)R_R + L_M R_s} \tag{5.51b}$$
$$\theta_1 = -\frac{1}{\tau_r+\tau_s} = -\frac{R_R R_s}{(L_\sigma+L_M)R_R + L_M R_s}. \tag{5.51c}$$

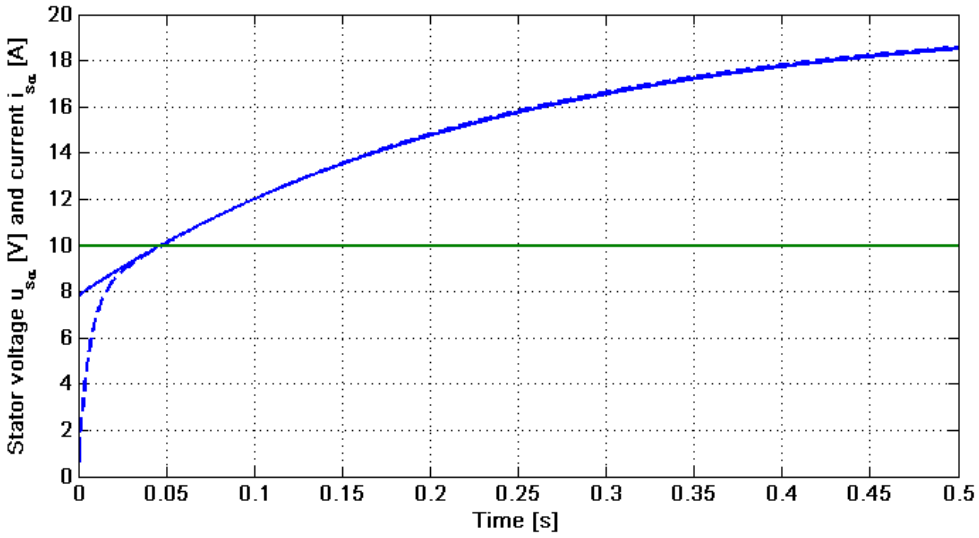

Figure 5.6: Simulated stator current response to a step voltage excitation. The simulated current is plotted with a dashed line ($--$) and the approximation with a solid line ($-$). Motor time constants are $\tau_s = 144.6$ ms, $\tau_r = 92.9$ ms, and the leakage factor is $\sigma \approx 0.10$.

The measurements should be taken after the initial transient is over in the real stator current (5.44), and stopped before the steady state is reached as Equation (5.47) is not valid at the beginning. In fact, the ideal stator current (5.44) is neither valid at the beginning as the initial transient has a high-frequency content causing nonlinear increase in the rotor parameters due to the skin effect. Therefore, the measurement should be started after, for example, three transient time constants τ_s' have passed from the beginning, yielding that the initial transient is practically over ($1 - \mathrm{e}^3 \approx 0.950$). The measurement can be stopped when the current has reached, for example, 93% of the steady state value corresponding to approximately four rotor time constants τ_r in Equation (5.47), i.e. ($1 - 0.5 \cdot \mathrm{e}^2 \approx 0.932$).

The parameters θ_0 and θ_1 can be solved from a matrix equation

$$\begin{bmatrix} 1 & t_1 \\ 1 & t_2 \end{bmatrix} \begin{bmatrix} \theta_0 \\ \theta_1 \end{bmatrix} = \begin{bmatrix} y(t_1) \\ y(t_2) \end{bmatrix} \tag{5.52}$$

as

$$\begin{bmatrix} \theta_0 \\ \theta_1 \end{bmatrix} = \frac{1}{t_2 - t_1} \begin{bmatrix} t_2 y(t_1) - t_1 y(t_2) \\ y(t_2) - y(t_1) \end{bmatrix}. \tag{5.53}$$

Finally, the transformed magnetizing inductance and rotor resistance can be solved

$$\widehat{L}_M = -\left(\widehat{L}_\sigma + \frac{\mathrm{e}^{\theta_0}}{\theta_1} \widehat{R}_s \right) \tag{5.54a}$$

$$\widehat{R}_R = \frac{1}{1 - \mathrm{e}^{\theta_0}} \left(\theta_1 \widehat{L}_\sigma + \mathrm{e}^{\theta_0} \widehat{R}_s \right). \tag{5.54b}$$

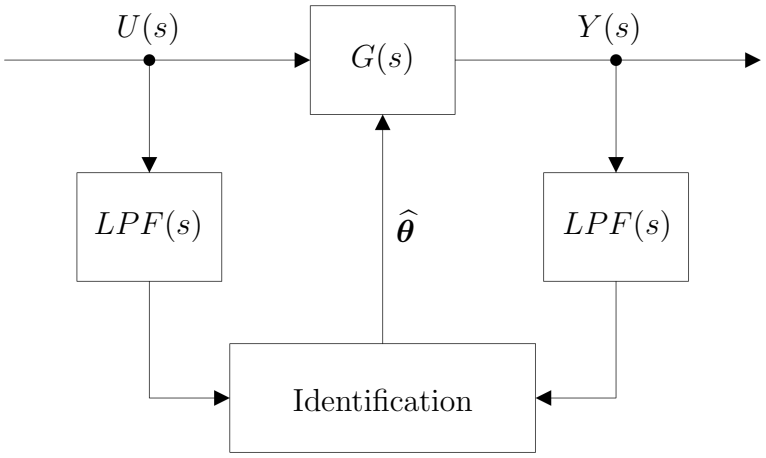

Figure 5.7: State variable filtering of an unknown process.

In practice, more than two measurements points should be taken so that the obtained parameters were not affected so much by noise or single wrong measurements.

5.7 Identification with State Variable Filtering

In the previous section, it was assumed that the stator resistance and the total leakage inductance were known in advance. However, those can be identified at the same time with the transformed rotor resistance and magnetizing inductance by identifying the whole model (5.38) at once.

This goal can be achieved if the system is identified with a method called state variable filtering (SVF). The method is capable of identifying any *linear* time-invariant system. The basic principle is to find the system's state variables by means of filtering the inputs and outputs (Garnier and Young, 2004). Figure 5.7 illustrates the case. The method uses continuous-time models. Thus, there is no need to discretize the identified model as it, usually, has been the case in the reviewed literature, e.g. in (Moon and Keyhani, 1993) and (Ruff and Grotstollen, 1996). This is advantageous as the accuracy of the identified parameters is not affected by the chosen discretization method. Moreover, time-discrete parameters have little or no physical meaning at all whereas the continuous-time parameters are directly mapped to the physical parameters. Furthermore, the SVF method does not need anti-aliasing filters, and the method works with arbitrary input signals (Johansson, 1993).

The SVF method goes as follows:

1. The Laplace variable s in a system's transfer function

$$G(s) = \frac{Y(s)}{U(s)} = \frac{b_1 s^{n-1} + \ldots + b_n}{s^n + a_1 s^{n-1} + \ldots + a_n} \tag{5.55}$$

is replaced by

$$s = \frac{1-\lambda}{\tau\lambda} \tag{5.56}$$

where λ is the new 'low-pass filter' operator and τ the low-pass filter time constant, which should be smaller than, or equal to, the lowest time constant of the identified system, i.e. the filter bandwidth should be higher than, or equal to, that of the identified system.

2. The new system

$$G(\lambda) = \frac{Y(\lambda)}{U(\lambda)} = \frac{\beta_n\lambda^n + \ldots + \beta_2\lambda^2 + \beta_1\lambda}{\alpha_n\lambda^n + \ldots + \alpha_2\lambda^2 + \alpha_1\lambda + 1} \tag{5.57}$$

is rearranged to the input-output model similar to autoregressive moving average

$$\begin{aligned} Y(\lambda) = &- \alpha_1\lambda Y(\lambda) - \alpha_2\lambda^2 Y(\lambda) - \ldots - \alpha_n\lambda^n Y(\lambda) \\ &+ \beta_1\lambda U(\lambda) + \beta_2\lambda^2 U(\lambda) + \ldots + \beta_n\lambda^n U(\lambda). \end{aligned} \tag{5.58}$$

3. The input-output model is transformed back to time domain with inverse Laplace transformation

$$\begin{aligned} y(t) = &- \alpha_1 \left[\lambda y\right](t) - \alpha_2 \left[\lambda^2 y\right](t) - \ldots - \alpha_n \left[\lambda^n y\right](t) \\ &+ \beta_1 \left[\lambda u\right](t) + \beta_2 \left[\lambda^2 u\right](t) + \ldots + \beta_n \left[\lambda^n u\right](t) \end{aligned} \tag{5.59}$$

where $\left[\lambda^i u\right](t)$ and $\left[\lambda^i y\right](t)$ are the ith-order low-pass filtered system inputs and outputs, respectively.

4. Finally, the obtained input-output description (5.59) is solved, for example, by means of a recursive least-squares algorithm described in Appendix A.

Applying the SVF to the Motor Model

The forthcoming application of the SVF method to the induction motor is essentially a simplification of the method that is used for real-time identification in (Dell'Aquila et al., 1994), but here the method is applied to the case where the rotor is not allowed to rotate.

First, the motor standstill model (5.38) is rearranged to the form (5.55)

$$G_1(s) = \frac{\dfrac{1}{\sigma\tau_s R_s}s + \dfrac{1}{\sigma\tau_r\tau_s R_s}}{s^2 + \dfrac{1}{\sigma}\left(\dfrac{1}{\tau_r} + \dfrac{1}{\tau_s}\right)s + \dfrac{1}{\sigma\tau_r\tau_s}} = \frac{b_1 s + b_2}{s^2 + a_1 s + a_2}. \tag{5.60}$$

Then, (5.56) is substituted for s

$$G(\lambda) = \frac{Y(\lambda)}{U(\lambda)} = \frac{(b_2\tau - b_1)\,\tau\lambda^2 + b_1\tau\lambda}{(1 - a_1\tau + a_2\tau^2)\,\lambda^2 + (a_1\tau - 2)\,\lambda + 1} = \frac{\beta_2\lambda^2 + \beta_1\lambda}{\alpha_2\lambda^2 + \alpha_1\lambda + 1} \tag{5.61}$$

which is solved for $Y(\lambda)$ and transformed back to the time domain

$$\begin{aligned} y(t) &= -\alpha_1\left[\lambda y\right](t) - \alpha_2\left[\lambda^2 y\right](t) + \beta_1\left[\lambda u\right](t) + \beta_2\left[\lambda^2 u\right](t) \\ &= \begin{bmatrix} -\left[\lambda y\right](t) & -\left[\lambda^2 y\right](t) & \left[\lambda u\right](t) & \left[\lambda^2 u\right](t) \end{bmatrix} \begin{bmatrix} \alpha_1 \\ \alpha_2 \\ \beta_1 \\ \beta_2 \end{bmatrix} = \boldsymbol{\varphi}^T\boldsymbol{\theta}. \end{aligned}$$

For convenience, the filtered inputs and outputs and the parameters are replaced with a simpler notation similar to the one commonly used in linear regression

$$\boldsymbol{\varphi} = \begin{bmatrix} -\left[\lambda y\right](t) \\ -\left[\lambda^2 y\right](t) \\ \left[\lambda u\right](t) \\ \left[\lambda^2 u\right](t) \end{bmatrix} = \begin{bmatrix} u_1(t) \\ u_2(t) \\ u_3(t) \\ u_4(t) \end{bmatrix} \qquad \boldsymbol{\theta} = \begin{bmatrix} \alpha_1 \\ \alpha_2 \\ \beta_1 \\ \beta_2 \end{bmatrix} = \begin{bmatrix} \theta_1 \\ \theta_2 \\ \theta_3 \\ \theta_4 \end{bmatrix}. \tag{5.62}$$

As was mentioned before, the motor can be excited with a voltage having an arbitrary waveform. For simplicity, the windings are excited again with the same step voltage that was used in Section 5.6. Both the estimated voltage and measured current are gathered into vectors

$$\mathbf{Y} = \begin{bmatrix} i_{s\alpha}(t_1) \\ i_{s\alpha}(t_2) \\ \vdots \\ i_{s\alpha}(t_N) \end{bmatrix} \quad \text{and} \quad \mathbf{U} = \begin{bmatrix} u_{s\alpha}(t_1) \\ u_{s\alpha}(t_2) \\ \vdots \\ u_{s\alpha}(t_N) \end{bmatrix}. \tag{5.63}$$

Discretized First-order Infinite Impulse Response Low-pass Filter

The filtered system inputs and outputs are obtained using a first-order infinite impulse response (IIR) low-pass filters. The discretization can be performed in various ways (Franklin et al., 1990). Hera, a zero-order hold and triangle-hold equivalents are presented:

- The zero-order hold equivalent

$$y_f(kh) = \mathrm{e}^{-h/\tau} y_f(kh - h) + \left(1 - \mathrm{e}^{-h/\tau}\right) u_f(kh - h) \tag{5.64}$$

- The triangle-hold equivalent

$$\begin{aligned} y_f(kh) = \mathrm{e}^{-h/\tau} y_f(kh - h) + \frac{\tau}{h}\Bigg[&\left(\frac{h}{\tau} - 1 + \mathrm{e}^{-h/\tau}\right) u_f(kh) \\ &+ \left(1 - \mathrm{e}^{-h/\tau} - \frac{h}{\tau}\mathrm{e}^{-h/\tau}\right) u_f(kh - h)\Bigg] \end{aligned} \tag{5.65}$$

where h is the inverse of the sampling frequency f_s, which should be chosen higher than the system bandwidth. However, too high a value causes numerical instabilities.

In practice, finite impulse response (FIR) filters may be preferred because such filters are faster to execute in digital signal processors, and because IIR filters may cause oscillations when implemented with fixed-point arithmetics (Niiranen, 1999). In addition, FIR filters can be designed with completely linear phase response. Further information on digital filters can be found in (Smith, 2003).

Recursive Identification

The parameter vector $\widehat{\boldsymbol{\theta}}$ is solved by means of recursive least-squares algorithm:

STEP 1. Choose the number of measurement points N, and the proper values for the filter time constant τ, forgetting factor μ and the covariance matrix gain α, see Appendix A.

STEP 2. Calculate the initial values for $\widehat{\boldsymbol{\theta}}$ and $\mathbf{P}$ or initialize them as

$$\widehat{\boldsymbol{\theta}}(0) = \begin{bmatrix} 0 \\ 0 \\ 0 \\ 0 \end{bmatrix}, \qquad \mathbf{P}(0) = \begin{bmatrix} \alpha & 0 & 0 & 0 \\ 0 & \alpha & 0 & 0 \\ 0 & 0 & \alpha & 0 \\ 0 & 0 & 0 & \alpha \end{bmatrix}.$$

STEP 3. Calculate the filtered inputs and outputs with, for example, (5.64).

STEP 4. Calculate the update coefficient

$$g_i(N) = \sum_{j=1}^{4} p_{ij}(N) u_j(N+1), \qquad i = \{1, 2, 3, 4\},$$

$$\boldsymbol{\gamma}(N) = \begin{bmatrix} \gamma_1(N) \\ \gamma_2(N) \\ \gamma_3(N) \\ \gamma_4(N) \end{bmatrix} = \frac{1}{\sum_{i=1}^{4} u_i(N+1) g_i(N) + \mu} \begin{bmatrix} g_1(N) \\ g_2(N) \\ g_3(N) \\ g_4(N) \end{bmatrix}.$$

STEP 5. Calculate the parameter estimate

$$e(N+1) = y(N+1) - \sum_{i=1}^{4} \theta_i(N) u_i(N+1),$$

$$\widehat{\boldsymbol{\theta}}(N+1) = \begin{bmatrix} \theta_1(N) + \gamma_1(N) e(N+1) \\ \theta_2(N) + \gamma_2(N) e(N+1) \\ \theta_3(N) + \gamma_3(N) e(N+1) \\ \theta_4(N) + \gamma_4(N) e(N+1) \end{bmatrix}.$$

STEP 6. Calculate the estimate for the covariance matrix

$$p_{ij}(N+1) = \frac{1}{\mu}\left(p_{ij}(N) - \gamma_i(N)\sum_{l=1}^{4} p_{lj}(N)u_l(N+1)\right), \qquad j = \{1,2,3,4\},$$

$$\mathbf{P}(N+1) = \begin{bmatrix} p_{11}(N+1) & p_{12}(N+1) & p_{13}(N+1) & p_{14}(N+1) \\ p_{21}(N+1) & p_{22}(N+1) & p_{23}(N+1) & p_{24}(N+1) \\ p_{31}(N+1) & p_{32}(N+1) & p_{33}(N+1) & p_{34}(N+1) \\ p_{41}(N+1) & p_{42}(N+1) & p_{43}(N+1) & p_{44}(N+1) \end{bmatrix}.$$

STEP 7. Stop if no more measurements, else go back to STEP 3.

Parameter Mappings

After the parameter vector (5.62) has been identified, the desired motor parameters are simply calculated from

$$\widehat{L}_\sigma = \frac{\tau}{\beta_1} \tag{5.66a}$$

$$\widehat{R}_s = \frac{1+\alpha_1+\alpha_2}{\beta_1+\beta_2} \tag{5.66b}$$

$$\widehat{L}_M = \frac{2+\alpha_1-\beta_1\widehat{R}_s}{\beta_1+\beta_2}\tau - \widehat{L}_\sigma \tag{5.66c}$$

$$\widehat{R}_R = \frac{\beta_1+\beta_2}{\tau^2}\widehat{L}_M\widehat{L}_\sigma. \tag{5.66d}$$

5.8 Frequency Response Identification

The time domain identification in the previous sections was based on feeding the stator windings with voltage or current pulses, which, by the definition of the Fourier transform, contain infinitely many frequencies with decaying amplitudes whereas the standstill frequency response (SSFR) identification methods are based on sinusoidal voltages and currents with constant amplitudes and frequencies. Thus, the system is excited with only one frequency at a time, and therefore it is easier to avoid exciting unwanted frequency dependent phenomenon.

The SSFR method has several advantages. For example, it is very accurate when performed with correlation method of frequency response (CMFR), which has a low computational burden and it gives good results even with poor signal-to-noise ratios. In addition, constant disturbances, like measurement offsets, are completely eliminated from the results.

On the other hand, identification takes more time with the SSFR method as it is necessary to wait for a certain period of time after changing the input frequency from one to another so that the initial transients have decayed enough. Furthermore, several periods have to be measured. Otherwise, the results are affected by

measurement noise. Recently, SSFR methods have successfully been applied to induction motors by Bünte and Grotstollen (1993), Sonnaillon et al. (2007) and Kwon et al. (2008).

The basis of the SSFR identification can be deduced from the way the motor currents divide between the stator and rotor circuits in steady-state conditions. When the rotor is at standstill, the magnetizing and rotor currents are related to the stator current by

$$I_M = \frac{1}{\sqrt{1 + (\omega_1 \tau_r)^2}} I_s \tag{5.67a}$$

$$I_R = \frac{\omega_1 \tau_r}{\sqrt{1 + (\omega_1 \tau_r)^2}} I_s. \tag{5.67b}$$

The magnitude of the magnetizing current I_M approaches zero as the stator frequency approaches infinity. Therefore, the AC current will entirely flow in the rotor. On there hand, when the stator frequency approaches zero, the magnitude of the rotor current I_R approaches zero, which means that the AC current will entirely flow in the stator circuit. Thus, the stator and rotor parameters can be solved form the stator impedance (3.22) when both low and high frequencies are used.

The parameters, L_σ, L_M and R_R, should be identified from the effective stator inductance

$$L_e(\omega_1) = L_\sigma + \frac{L_M}{1 + (\omega_1 \tau_r)^2} \tag{5.68}$$

as it is not affected by the stator resistance nor the nonlinear inverter resistance $R_i(\underline{i}_s)$, introduced in Section 5.2. There is a problem however. As the motor is not supplied with a symmetrical sinusoidal three-phase supply, the input power is not constant because the amplitudes of the current and voltage space vectors pulsate with the stator frequency. As a consequence, the information of the phase angle vanishes every time a space vector becomes zero.

The inductance could be calculated recursively by solving a discretized version of the stator voltage equation

$$u_{s\alpha}(t) = R_e i_{s\alpha}(t) + L_e \frac{\mathrm{d}i_{s\alpha}(t)}{\mathrm{d}t} \tag{5.69}$$

as is done in (Bertoluzzo et al., 1997) and (Aiello et al., 2002). However, solving the resulting discrete autoregressive moving average has the same disadvantages that were discussed in the beginning of Section 5.7.

Fortunately, there is a better way. The effective stator inductance can be solved from the reactive input power (3.25c)

$$L_e(\omega_1) = \frac{u_{s\alpha}}{i_{s\alpha}} \cdot \frac{\sin(\varphi_1)}{\omega_1}. \tag{5.70}$$

if only the phase difference φ_1 between the fundamental-frequency voltage and current *phasors* is known. This information is easily obtained using the correlation method of frequency response presented next.

Correlation Method of Frequency Response

The correlation method of frequency response (CMFR) is the basic tool in discrete Fourier transform as it has an ability to find the amplitude ratio and phase difference between any two sinusoidal signals. The method is usually exploited in phase-locked loops (PLL) and lock-in amplifiers (LIA) used in signal tracking applications. For example, the motor identification method presented in (Sonnaillon et al., 2007) uses this technique, although different name is used.

A simple derivation of the method is presented below for a general sampled system, whose input and output signals, $u(kh)$ and $y(kh)$, are defined as

$$u(kh) = \hat{u}\sin(\omega_1 kh) \tag{5.71a}$$

$$\begin{aligned} y(kh) &= \hat{y}\sin(\omega_1 kh + \varphi_1) \\ &= \hat{y}_c\cos(\omega_1 kh) + \hat{y}_s\sin(\omega_1 kh)\,. \end{aligned} \tag{5.71b}$$

whereas the amplitudes, $\hat{y}$, $\hat{y}_c$ and $\hat{y}_s$, are

$$\hat{y} = \sqrt{\hat{y}_c^2 + \hat{y}_s^2} \tag{5.72a}$$

$$\hat{y}_c = \hat{y}\sin(\varphi_1) \tag{5.72b}$$

$$\hat{y}_s = \hat{y}\cos(\varphi_1)\,. \tag{5.72c}$$

Now, the system gain $K(\omega_1)$ and phase difference $\varphi_1(\omega_1)$ can be obtained from

$$K(\omega_1) = \left|G(\mathrm{e}^{\mathrm{j}\omega_1 h})\right| = \frac{\hat{y}}{\hat{u}} \tag{5.73a}$$

$$\varphi_1(\omega_1) = \arctan\left(\frac{\hat{y}_c}{\hat{y}_s}\right) \tag{5.73b}$$

if only the coefficients $\hat{y}_c$ and $\hat{y}_s$ are known.

Basically, the output signal is separated into components having 90-degree phase shifts between each other by multiplying the output signal with a cosine and sine having the same frequency f_1 as the input signal. Then, both components are integrated over a measuring interval t_m chosen as an integer multiple l of the period t_1 of the input frequency

$$t_m = lt_1 = l\frac{2\pi}{\omega_1}, \quad l \in \{1, 2, \ldots\}\,. \tag{5.74}$$

During that time, N measurement points are taken from the output signal with a sampling frequency $f_s = \frac{1}{h}$

$$N = t_m f_s + 1 = \frac{t_m}{h} + 1. \tag{5.75}$$

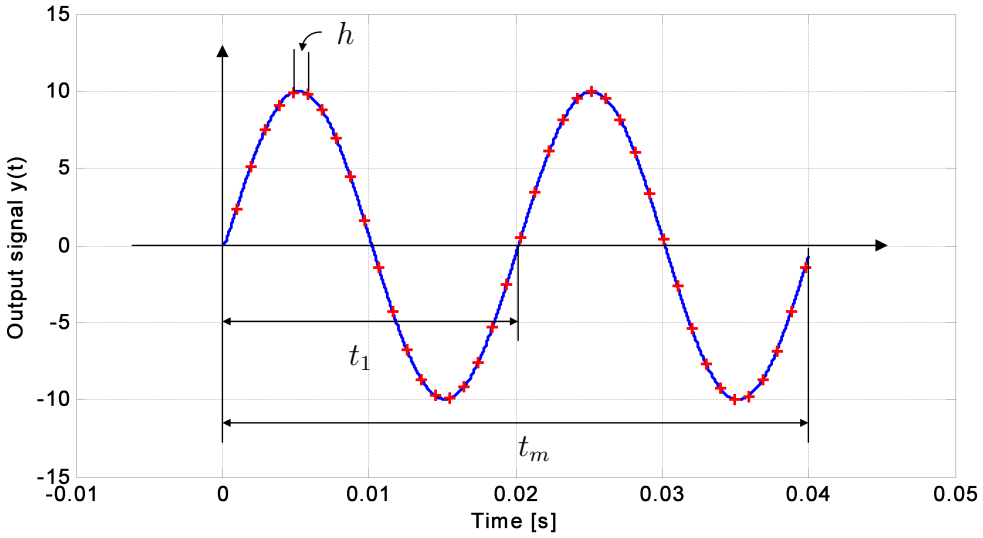

Figure 5.8: Measured signal in the correlation method of frequency response.

Figure 5.8 illustrates the sampling process. In discrete time, the integrals are replaced with the corresponding sums. As a consequence, the coefficients can be calculated from

$$\hat{y}_c = \frac{2}{N} \sum_{k=0}^{N-1} y(kh) \cos(\omega_1 kh) \tag{5.76a}$$

$$\hat{y}_s = \frac{2}{N} \sum_{k=0}^{N-1} y(kh) \sin(\omega_1 kh) \,. \tag{5.76b}$$

More thorough derivation of the method can be found in (Franklin et al., 1990, p. 354).

SSFR Identification Process

The stator windings are fed with a combination of DC and AC currents

$$i_{s\alpha}(t) = I_{dc} + \sqrt{2} I_{ac} \sin(\omega_1 t) \,. \tag{5.77}$$

The purpose of the DC component I_{dc} is to magnetize the motor in a desired operation point, and to minimize the nonlinear change in magnetization caused by the magnetic hysteresis and saturation otherwise present when the motor is magnetized with a sinusoidal current alone. Furthermore, the added DC component can be used to excite the motor above the nonlinear inverter region if it is a problem, see Figure 5.2.

In the following, the DC component is chosen as the nominal magnetizing current and the angular frequency of the sine wave as the nominal ω_{1N}. Now, the total

leakage inductance can be solved from the effective stator inductance (5.70) as they are approximately equal in this operation point

$$\widehat{L}_\sigma \approx L_e(\omega_{1N}). \tag{5.78}$$

To identify the transformed magnetizing inductance L_M and rotor resistance R_R, the motor has to be fed again with the above combination of DC and AC currents, but this time the effective stator inductance must be measured with at least two different stator frequencies. These two frequencies are chosen from the low-frequency end, close to the nominal angular slip frequency ω_{2N}.

An estimate for the proper stator current that will cause the nominal magnetizing current at low frequencies can be obtained from the displacement power factor

$$I_{MN} \approx I_N \sin\varphi_N = I_N\sqrt{1-(\cos\varphi_N)^2} \tag{5.79a}$$

$$I_{RN} \approx I_N \cos\varphi_N \tag{5.79b}$$

where I_{MN} and I_{RN} are the magnetizing and rotor currents with nominal stator current, respectively. Then, the correct stator current is obtained from Equation (5.67a)

$$I_s(\omega_1) = \sqrt{1+(\omega_1\widehat{\tau}_r)^2}I_{MN} \tag{5.80}$$

where the rotor time constant is estimated from the motor name-plate (5.14).

After the measurements have been taken, the transformed magnetizing inductance can be solved from a linear 2×2 system

$$\frac{1}{L_e(\omega_a)-\widehat{L}_\sigma}\widehat{L}_M - \omega_a^2\widehat{\tau}_r^2 = 1 \tag{5.81a}$$

$$\frac{1}{L_e(\omega_b)-\widehat{L}_\sigma}\widehat{L}_M - \omega_b^2\widehat{\tau}_r^2 = 1 \tag{5.81b}$$

where ω_a and ω_b are the different angular measurement frequencies. The transformed rotor resistance is then easily solved from the estimate of the rotor time constant

$$\widehat{R}_R = \frac{\widehat{L}_M}{\widehat{\tau}_r}. \tag{5.82}$$

5.9 Magnetizing Curve Identification

If the motor is going to be operated above the rated speed n_N with reduced rotor flux linkage, or if more torque is wanted with less current, or if the magnetic circuit is too nonlinear, a constant value for the magnetizing inductance is inadequate for good control performance. In such conditions, the saturation curve has to be known for the rotor flux linkage or the magnetizing inductance. Such curves are depicted in

Figures 5.9 and 5.10. Unfortunately, the task of finding these curves is the hardest part in standstill identification as several tests have to be performed, and as the process is complicated at low voltages by the inverter nonlinearity and magnetic hysteresis, particularly when step response tests are used. Therefore, only a short introduction to one method is presented below as a thorough discussion of the topic is beyond the scope of this Master's thesis.

The magnetizing inductance is divided into static and dynamic parts where the former is defined as the slope of the straight line drawn from the origin to a particular operating point in the curve of the rotor flux linkage versus the magnetizing current

$$L_M(\underline{i}_M) = \frac{\left|\underline{\psi}_R(\underline{i}_M)\right|}{|\underline{i}_M|} \tag{5.83}$$

whereas the latter is the slope of the tangent at that point

$$L_D(\underline{i}_M) = \frac{\mathrm{d}\left|\underline{\psi}_R(\underline{i}_M)\right|}{\mathrm{d}\,|\underline{i}_M|} \tag{5.84a}$$

$$= L_M(\underline{i}_M) + \frac{\mathrm{d}L_M(\underline{i}_M)}{\mathrm{d}\,|\underline{i}_M|}\ |\underline{i}_M|\,. \tag{5.84b}$$

The problem is to find a smooth function that accurately estimates the static magnetizing inductance. For example, Ruff and Grotstollen (1996) have used an exponent function

$$\widehat{L}_M(\underline{i}_M) = L_a\,\mathrm{e}^{K_a\ |\underline{i}_M|} + L_b\,\mathrm{e}^{K_b\ |\underline{i}_M|} + L_c \tag{5.85}$$

where the parameters L_a and L_c are positive, and L_b, K_a and K_b negative. As the above equation is nonlinear with respect to the parameters, it cannot be solved with linear regression, which means that a very time-consuming numerical optimization should be used. Therefore, other simpler functions are preferred in literature.

Yet, single values for the static magnetizing inductance can still be solved rather easily by combining the flux linkage equations (3.16), the stator voltage equation (3.17a) and the nonlinear inverter resistance (5.20b). It follows that the rotor flux linkage can be obtained from

$$\psi_{R\alpha}(t) = \psi_{R\alpha}(0) + \int_0^t \Big[u_{s\alpha,ref}(t') - \widehat{R}_{ei}\big(i_{s\alpha}(t')\big)\, i_{s\alpha}(t')\Big]\mathrm{d}t' - \widehat{L}_\sigma i_{s\alpha}(t) \tag{5.86}$$

where the initial value $\psi_{R\alpha}(0)$ exists due to the magnetic hysteresis. Equation (3.16c) yields an expression for the magnetizing inductance

$$\widehat{L}_M(i_{s\alpha,i}) = \left.\frac{\psi_{R\alpha,i}(t)}{i_{M\alpha,i}(t)}\right|_{t\to\infty} = \left.\frac{\psi_{R\alpha,i}(t)}{i_{s\alpha,i}(t)}\right|_{t\to\infty} \qquad i \in \{0, 1, 2, \ldots\} \tag{5.87}$$

where the last equality holds if the motor is fed with constant DC voltages, in which case the steady-state stator current equals the steady-state magnetizing current.

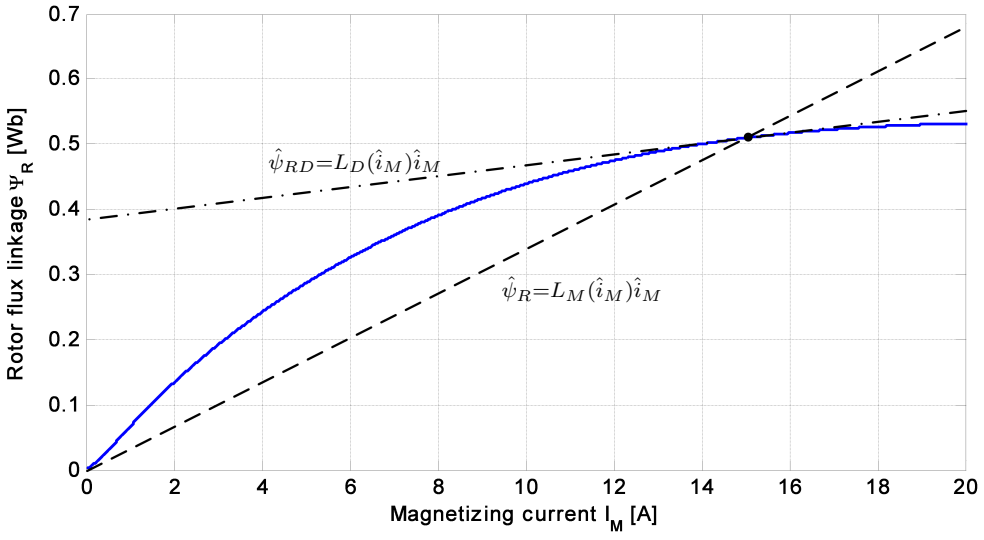

Figure 5.9: Rotor flux linkage as a function of the magnetizing current.

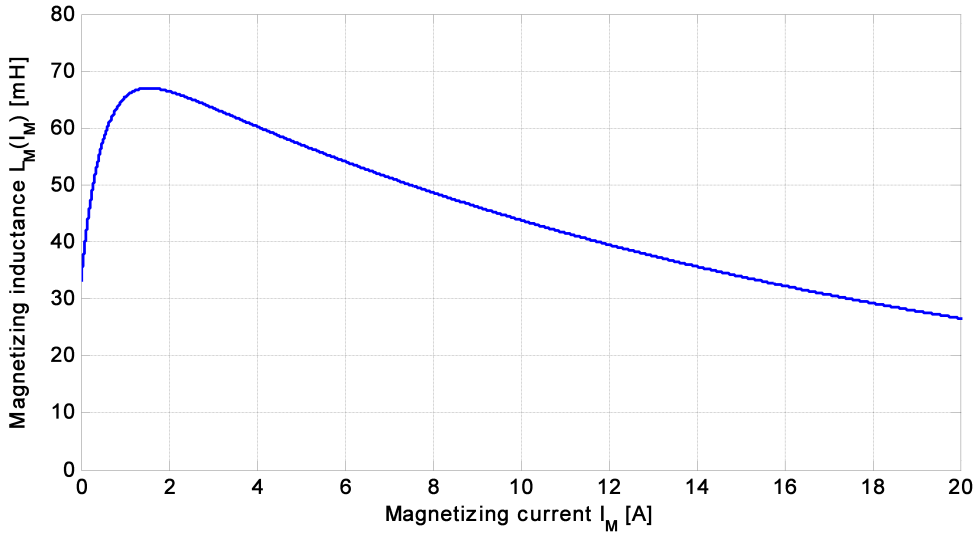

Figure 5.10: Static magnetizing inductance as a function of the magnetizing current.

After those single values are solved for the magnetizing inductance, the real magnetizing curve can be approximated using linear interpolation between two consecutive values.

More detailed information about the used method can be found in (Ruff and Grotstollen, 1996) and (Sukhapap and Sangwongwanich, 2002), and a comparison of different types of functions that have been used for estimating the static magnetizing inductance in (Ganji et al., 1996). Methods based on SSFR can be found in (Bünte and Grotstollen, 1993), (Sonnaillon et al., 2007).

6 Simulation Results

An ideal induction motor without any nonlinearities was identified with both the step and frequency response methods using simulated input-output data. The simulations were performed with MATLAB Simulink, which is a numerical computing environment produced by Mathworks. The motor parameters are $\widehat{L}_\sigma = 7.3$ mH, $\widehat{R}_s = 0.5\ \Omega$ and $\widehat{L}_M = 65.0$ mH and $\widehat{R}_R = 0.7\ \Omega$, which yield the following time constants: $\tau_s' = 6.1$ ms, $\tau_s = 144.6$ ms and $\tau_r = 92.9$ ms. That is, the two poles of the motor's standstill transfer function (5.38) are located at 0.7 Hz and 27.2 Hz.

Step Response Test with SVF

In the first simulation, the motor was fed with a voltage pulse shown in Figure 6.1 using '**Case 1**'-excitation, see Section 5.4. The pulse-duration was one second and it had an amplitude of 10 volts. The simulated voltage and current vectors were then processed by the state variable filtering method using the recursive identification algorithm presented in Section 5.7.

The algorithm was run several times with different values for the low-pass filter cut-off frequency f_0 and sampling frequency f_s. Then, a second test was performed similarly with an exception that bandwidth-limited white noise with 100 mA mean and 100 mA standard deviation was added to the stator current to model measurement noise and offset, see Figure 6.2. Results from both tests are presented in Table 6.1.

It is observed that the stator resistance is the only parameter that stays rather accurate regardless of the chosen filter cut-off frequency or the sampling frequency. Furthermore, it appears that the sampling frequency has least effect when the filter cut-off frequency is selected close to the lower pole. Moreover, it seems that over-sampling tends to increase inductances, which is probably caused by increasing numerical problems in the least-squares method, i.e. the input-output data does not have enough variations. All in all, the *chosen* level of measurement noise and offset has a very small effect on the estimated parameters. In general, the estimates are not that much affected by the white noise no matter how high compared to high levels of measurement offset.

There is also a fundamental problem in induction motor identification caused by the fact that the two poles are so far from each other in the frequency domain, which means that the lower pole, approximately corresponding to the L_M and R_R, should be identified with a lower filter cut-off frequency, and the higher pole, roughly corresponding to the L_σ, with a higher cut-off frequency. Thus, in this case, the values estimated with f_0 and f_s near 30 Hz and 5 kHz, respectively, are likely to be more correct for the L_σ than for the others, and vice versa when f_0 is near 1 Hz.

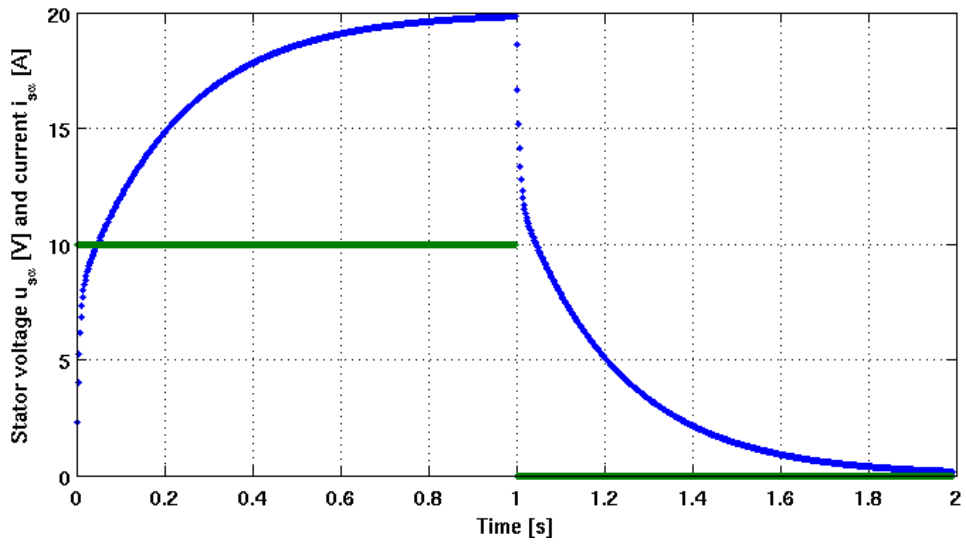

Figure 6.1: Stator current response to a step voltage excitation. $f_s = 500$ Hz.

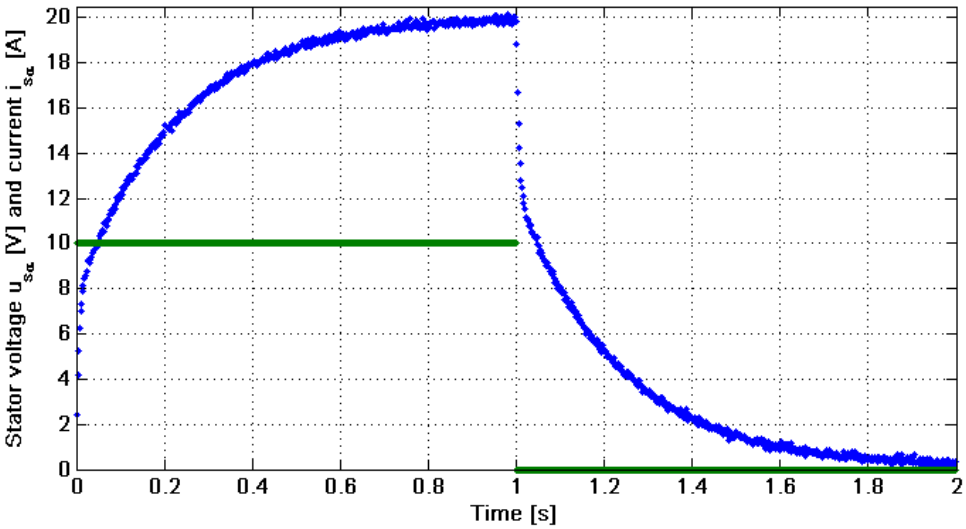

Figure 6.2: Stator current response to a step voltage excitation when measurement noise and offset are modeled. $f_s = 500$ Hz.

Table 6.1: Results from the first (-) and second (noise) step response test. f_0 is the filter cut-off frequency and f_s the sampling frequency.

[Hz]	[kHz]	$\widehat{L}_\sigma$ [mH]		$\widehat{R}_s$ [Ω]		$\widehat{L}_M$ [mH]		$\widehat{R}_R$ [Ω]	
f_0	f_s	-	noise	-	noise	-	noise	-	noise
1.0	10.0	8.1	9.1	0.50	0.50	72.2	72.0	0.70	0.66
5.0	10.0	8.1	8.1	0.50	0.50	72.1	72.6	0.70	0.69
30.0	10.0	8.1	7.9	0.50	0.50	71.5	71.2	0.70	0.71
50.0	10.0	8.0	7.8	0.50	0.50	71.0	70.7	0.70	0.72
100.0	10.0	7.9	7.3	0.50	0.50	69.9	62.6	0.71	0.88
500.0	10.0	7.1	2.4	0.50	0.53	62.1	42.0	0.76	9.23
1.0	5.0	7.7	9.0	0.50	0.50	68.3	68.0	0.70	0.65
5.0	5.0	7.7	7.7	0.50	0.50	68.2	68.7	0.70	0.69
30.0	5.0	7.6	7.5	0.50	0.50	67.1	67.4	0.71	0.71
50.0	5.0	7.5	7.3	0.50	0.50	66.2	65.4	0.71	0.73
100.0	5.0	7.3	6.5	0.50	0.51	64.2	55.2	0.72	0.98
500.0	5.0	6.2	2.4	0.51	0.53	51.3	33.8	0.84	9.77
1.0	1.0	7.6	9.0	0.50	0.50	65.2	64.7	0.70	0.64
5.0	1.0	7.4	7.4	0.50	0.50	64.5	65.1	0.70	0.68
30.0	1.0	6.9	6.8	0.50	0.50	59.8	59.7	0.73	0.74
50.0	1.0	6.7	6.3	0.50	0.50	56.4	53.9	0.76	0.83
100.0	1.0	6.2	4.9	0.51	0.52	49.1	39.1	0.85	1.40
500.0	1.0	3.9	2.3	0.53	0.53	16.6	12.5	1.91	7.63
1.0	0.5	8.1	9.8	0.50	0.50	64.3	63.6	0.69	0.62
5.0	0.5	7.8	7.8	0.50	0.50	62.9	63.4	0.69	0.68
30.0	0.5	6.9	6.7	0.50	0.50	54.2	53.8	0.73	0.75
50.0	0.5	6.5	5.9	0.50	0.50	48.6	45.5	0.76	0.86
100.0	0.5	5.5	4.5	0.51	0.52	37.3	29.4	0.87	1.41
500.0	0.5	1.8	1.4	0.52	0.53	9.5	6.8	1.22	3.30
Real		**7.3**		**0.5**		**65.0**		**0.7**	

Frequency Response Test with CMFR

As a first SSFR test, it was studied how accurately the CMFR method finds the total stator leakage inductance with and without measurement offset and noise when the ratio of the sampling frequency and the stator frequency was varied from 2.5 to 80. The measurement noise was modeled again as a bandwidth-limited white noise but this time a low signal-to-noise ratio, 5.1 dB, was used: standard deviation 2.23 A and mean 1.0 A. Furthermore, the measurement duration t_m was varied from one to three periods of f_1 to see how the averaging improves accuracy. Test results are presented in Table 6.2 and the input-output signals in Figure 6.3.

As was expected, the method found the correct value for the total stator leakage inductance very accurately even in the presence of heavy measurement noise and huge offset that would have ruined the estimate if the step response method were used. In fact, due to the method's characteristics, it is completely immune to measurement offsets. It was also rather surprising how well the CMFR method performed when only one period of test signals was measured in the noise-free case. Furthermore, the parameter accuracy was higher than expected even with very low sampling frequencies.

As a second SSFR test, the motor was fed again with the '**Case 1**'-excitation but this time three different test frequencies were used at a time: 50.0, 1.0 and 0.5 Hz. Moreover, the offset and noise were both reduced to a more reasonable value: 100 mA. The simulated voltage and current vectors were sampled with a frequency twenty times higher than that of the excitation, after which one period of test signals was removed from the beginning of both vectors to be sure that the initial transients were decayed enough. Then, both vectors were processed with the CMFR method whose measurement time was varied as in the first test. Results are presented in Table 6.3, and the signal waveform is plotted in the middle of Figure 6.3.

It is observed that the accuracy of the identified parameters is similar to those obtained from the step response test as the identified system was linear. In addition, the frequency response test took three to six times longer to complete than the step response test. However, the SSFR method has superior accuracy even with poor signal-to-noise ratios, and the identified parameters are less affected by the nonlinearities.

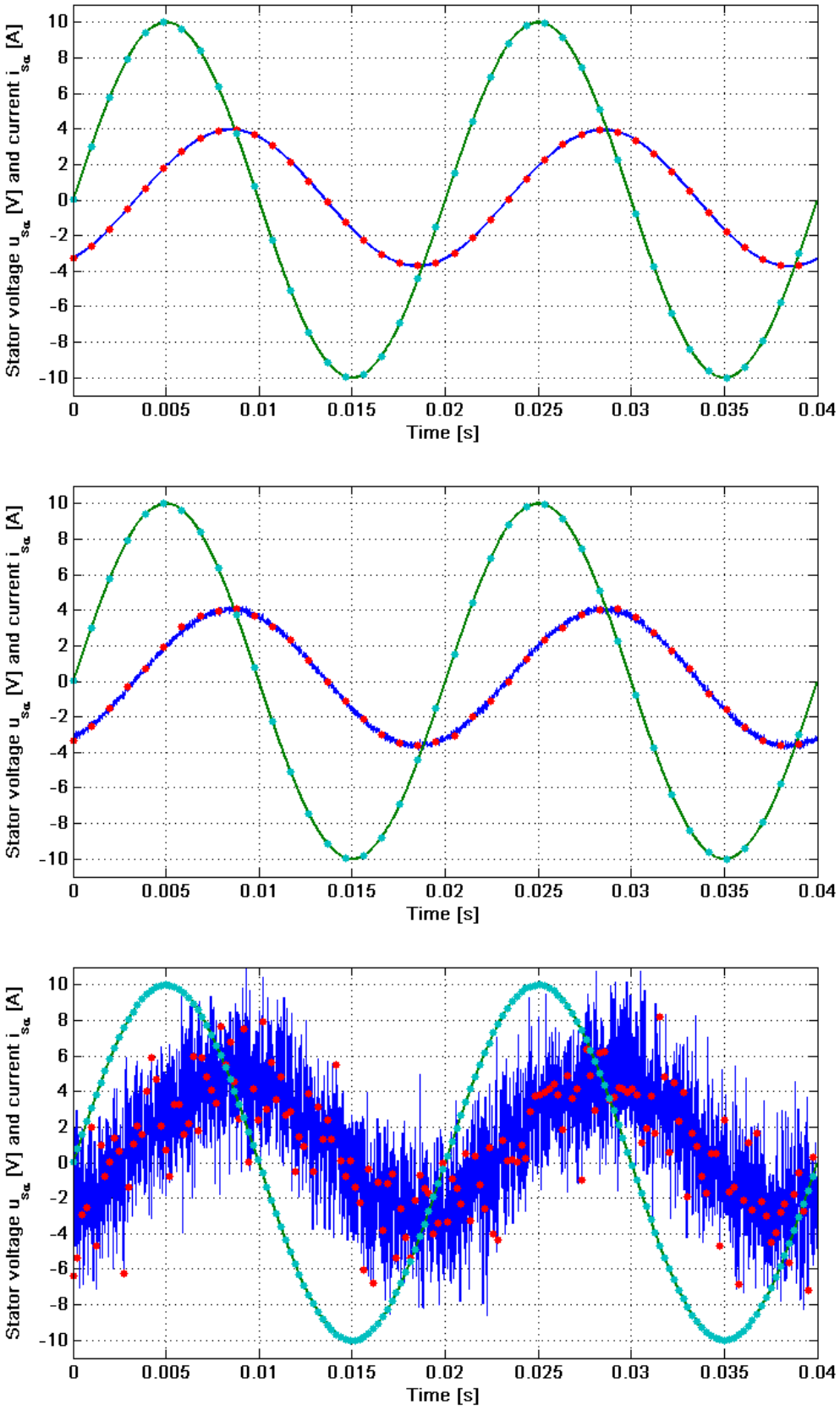

Figure 6.3: Current response to sinusoidal voltage excitation with and without measurement noise. Sampling frequency is $20f_1$ in the plots at the top and middle, and $80f_1$ in the one at the bottom.

Table 6.2: The effect of the chosen sampling frequency and test duration in the CMFR method. Initial transients are removed. Test frequency is 50.0 Hz. Measurement noise and offset are modeled as bandwidth-limited white noise with 1.0 A mean and 2.23 A standard deviation. Signal-to-noise ratio is approximately 5.1 dB.

	$\widehat{L}_\sigma$ [mH]					
	-			Offset + Noise		
f_s/f_1	t_1	$2t_1$	$3t_1$	t_1	$2t_1$	$3t_1$
80	7.4	7.4	7.4	8.5	7.4	7.8
40	7.5	7.4	7.4	6.9	6.7	7.3
20	7.7	7.5	7.5	11.8	6.4	7.8
10	8.1	7.8	7.6	9.0	8.3	7.3
5	7.9	7.5	7.5	8.5	5.5	4.1
2.5	7.5	4.2	7.6	6.7	3.4	6.5
2	0.0	0.0	0.0	0.0	0.0	0.0
Real	**7.3**					

Table 6.3: Results from the simulated standstill frequency response test. The effective stator inductance is measured at 50.0, 1.0 and 0.5 Hz. The level of noise and offset are reduced to 100 mA. t_m is the time used measuring one frequency. Σt_m is the total test duration. Sampling frequency is $f_s = 20 f_1$.

t_m	Σt_m [s]	$\widehat{L}_\sigma$ [mH]	$\widehat{L}_M$ [mH]	$\widehat{R}_R$ [Ω]
t_1	6.04	7.9	63.5	0.71
$2t_1$	9.06	7.5	64.5	0.70
$3t_1$	12.08	7.5	64.7	0.69
Real		**7.3**	**65.0**	**0.7**

7 Experimental Results

The studied identification methods were also investigated with experimental tests. A typical elevator motor was identified using the equipment listed in Table 7.1. The motor name-plate is given in Table 7.2.

The first parameter estimates were calculated from the name-plate, after which the motor was identified with a basic locked rotor and no-load tests (LRNL). Subsequently, the identification was performed with the step response method (SR), the state variable filtering method (SVF) and the frequency response method (FR) introduced in Sections 5.6, 5.7 and 5.8, respectively. The CMFR method was not used but the system gain and phase were measured with an oscilloscope.

In the SR and SVF tests, the motor was supplied with a DC power source, and the stator voltages were measured with differential high-voltage probes whereas the currents were measured with shunts. The measurements were recorded with a three-phase power analyzer, and processed in MATLAB. Figure 7.1 shows what happens to the current response when the magnetic circuit saturates, i.e. the slope of the current increases. Table 7.3 presents the results from the SVF test. Due to the magnetic hysteresis, the falling edge of the current response was not used in the calculations as it would have caused erroneous results.

In the LRNL and FR tests, the motor was supplied with a frequency converter. This time, the stator voltage and current measurements were fed through an analog 8th-order low-pass filter with a Butterworth response to extract the fundamental-frequency component from the pulse-width modulated stator voltage, and to keep both measurements equally delayed. Furthermore, in the FR test, the effect of hysteresis was minimized using constant magnetization with a DC component as was explained in Section 5.8.

From the results of Table 7.4, it is observed how the studied methods gave results that are rather close to each other, although the approaches were completely different. However, it might be just a lucky coincidence that the name-plate approximation was so accurate for this particular motor. The table also reveals how the parameters obtained from the step response methods are affected by the rotor-bar skin effect as the rotor resistances are almost two times higher than those from the LRNL and FR tests. However, the SVF based SR method managed to identify the transformed magnetizing inductance with almost the same accuracy as the FR method. Furthermore, the tests with only few measurements, like the SR test in this case, are very sensitive to measurement errors.

Table 7.1: Test equipment.

• KONE proprietary frequency converter
• Delta Elektronika Power Supply SM 70-90
• LEM Norma 5000 Power Analyzer
• Tektronix TDS3014 Oscilloscope
• Kemo VBF 8 Dual Variable Filter

Table 7.2: The name-plate of the tested induction motor Elemol CTF 160M.30R.

Power	7.5 kW
Rated voltage	340 V
Rated current	23 A
Power factor	0.8
Frequency	50 Hz
Rated speed	950 rpm
Rotor inertia	0.19 kgm^2

Table 7.3: Results from the experimental step response test.

f_0 [Hz]	f_s [kHz]	$\widehat{L}_\sigma$ [mH]	$\widehat{R}_s$ [Ω]	$\widehat{L}_M$ [mH]	$\widehat{R}_R$ [Ω]
1.0	5.0	9.4	0.48	65.1	0.87
5.0	5.0	8.0	0.48	66.8	0.89
30.0	5.0	7.3	0.48	65.5	0.94
1.0	1.0	9.4	0.48	65.1	0.87
5.0	1.0	8.0	0.48	66.1	0.89
30.0	1.0	7.1	0.48	61.1	0.97
1.0	0.5	9.7	0.48	64.6	0.85
5.0	0.5	8.1	0.48	64.9	0.87
30.0	0.5	7.1	0.48	56.4	1.00

Table 7.4: Experimental results from different identification tests.

Test method	Motor parameters				Notes
	$\widehat{L}_\sigma$ [mH]	$\widehat{R}_s$ [Ω]	$\widehat{L}_M$ [mH]	$\widehat{R}_R$ [Ω]	
Name-plate	6	0.7	62	0.7	$\widehat{R}_s \approx \widehat{R}_R$, $\widehat{L}_\sigma \approx 0.1\widehat{L}_M$
LRNL	6	0.48	67	0.7	50 Hz, 2.5 Hz
SR test	11	0.48	54	1.2	2 points
SVF	7.3	0.48	66	0.9	$f_0 = \{1.0, 30.0\}$ Hz, 5.5 V / 11.7 A
FR test	7.5	-	63	0.5	50, 2.5, 0.5 Hz

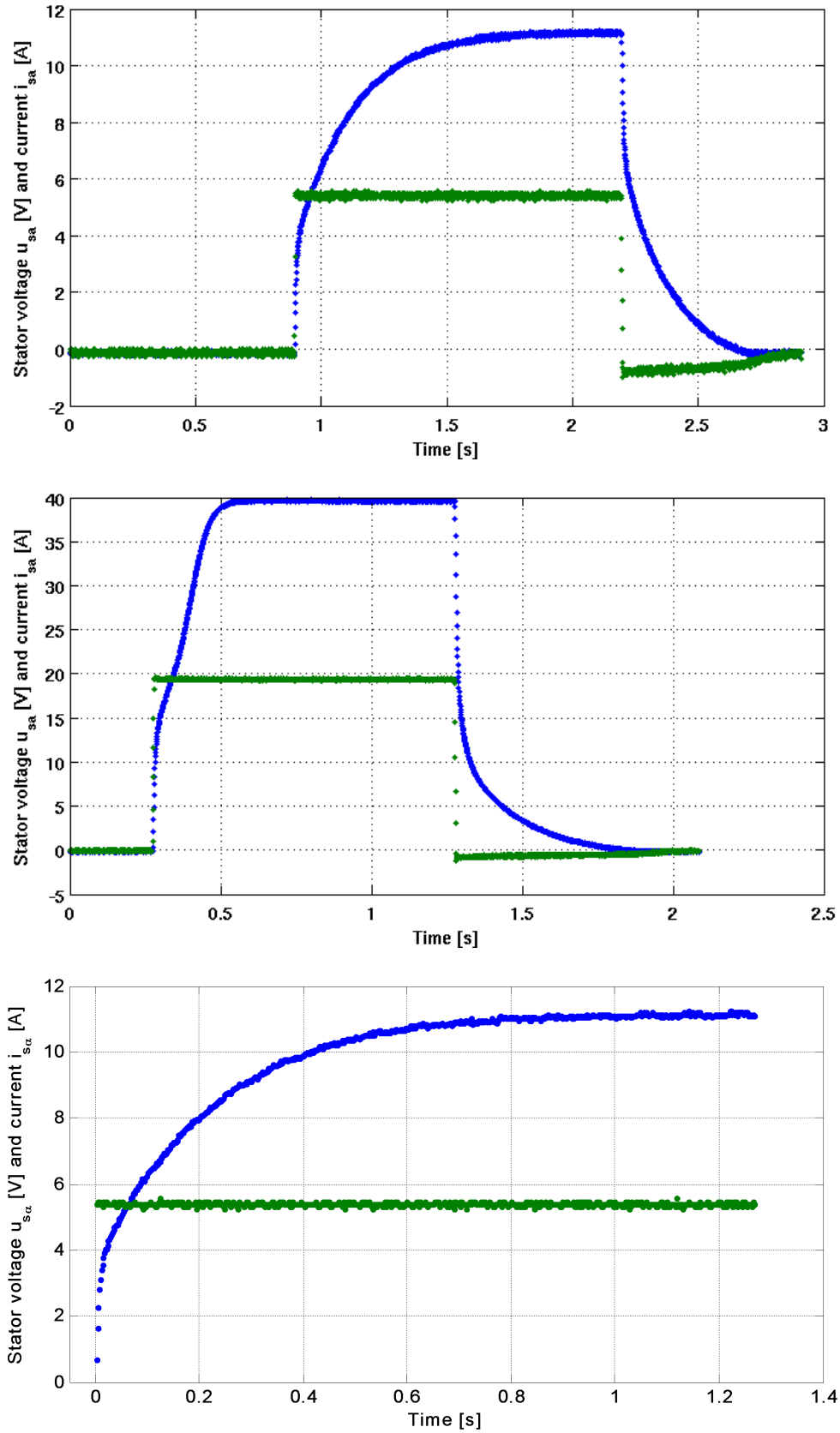

Figure 7.1: 'Unsaturated' (top) and saturated (middle) current responses to a step voltage excitation produced with a DC power supply. The figure bottom shows the data used in the SVF method to avoid hysteresis and saturation.

8 Conclusions

The object of this master's thesis was to find a method that could accurately identify the electrical parameters of the mathematical model of the induction motor that is powered with a frequency converter in a condition where the motor is not allowed to rotate. The identification was found possible if the motor is excited with such a three-phase voltage that does not produce torque. The desired parameters can then be solved from the resulting voltages and currents with system identification methods based on transient and frequency responses, respectively.

The identification process is complicated because neither the output voltage of the pulse-width modulated inverter nor the rotor currents of the induction motor with a squirrel-cage rotor can be measured. Thus, both variables have to be estimated from the commanded stator voltage and the measured stator current. However, the relationship between the two is nonlinear if the voltage drops caused by the transistors and the freewheeling diodes, and the reduced pulse-width caused by the dead-time are not compensated. Thus, if not taken into account, the aforementioned nonlinearity will act as an additional series resistance that cannot be separated from the motor's stator resistance without impractical phase voltage sensors.

In the studied transient response method, the stator windings were fed with a step voltage, whose magnitude was selected such that the resulting current did not cause magnetic saturation. The measured current and the estimated voltage were processed with a method called state variable filtering (SVF) that was applied to induction motor at standstill, and the produced linear system of equations was solved with recursive least-squares algorithm. The desired motor parameters were then calculated from the obtained parameter vector.

On the other hand, the studied frequency response method was based on the combination of DC and AC excitations. The DC component was used to set the desired level of magnetization while the AC component and the corresponding voltage were processed using the correlation method of frequency response. As a result, the system gain and phase difference were obtained at selected frequencies. This information was then used in calculating the input inductance, from which the other motor parameters were solved.

It was observed that the methods based on transient response were faster to conduct than those based on frequency response as the latter methods require several seconds, even minutes, to complete. However, the former methods produce incorrect results when applied to systems whose parameters change with frequency as the non-sinusoidal excitations used in such methods contain several frequencies. Therefore, methods with such excitations should not be used when identifying induction motors where the rotor resistance and leakage inductance change with frequency due to the skin and proximity effects, or else the results have to be corrected for such effects. According to author's opinion, frequency response methods should be used as then the obtained parameter accuracy is only restricted by the quality of the voltage estimation and current measurements. Moreover, more code has to be written if transient response methods are going to be implemented as such methods usually

require curve-fitting algorithms, e.g. recursive least-squares or maximum likelihood ones.

Although the transient response methods are not recommended when identifying the electrical parameters, they could be used to identify systems without frequency dependencies. For example, the SVF method could be modified to track variations in the mechanical parameters.

Furthermore, if the motor is going to be operated above the rated speed with reduced rotor flux linkage, or if more torque is wanted with less current, the magnetization curve should also be identified. The best method for this purpose is the frequency response one as then the parameter accuracy is not affected by that of stator resistance as it is the case with transient response methods.

If further investigations were conducted, it should be studied how the parameter variations could be tracked when the motor heats up. For example, model-reference adaptive system based estimators or the SVF method could be used for this purpose.

References

Aiello, M., Cataliotti, A., and Nuccio, S. (2002). "A fully-automated procedure for measuring the electrical parameters of an induction motor drive with rotor at standstill." In *19th IEEE Instrumentation and Measurement Technology Conference*, vol. 1, pp. 681–685.

Ambrožić, V., Cajhen, R., and Nastran, J. (1993). "A step voltage method for determination of an induction motor rotor time constant in cold state." *IEEE International Symposium on Industrial Electronics in Budapest*, pp. 85–89.

Ba-Razzouk, A., Chériti, A., and Sicard, P. (2002). "Implementation of a DSP based real-time estimator of induction motors rotor time constant." *IEEE Transactions on Power Electronics*, **17**(4), pp. 534–542.

Barrero, F., Pérez, J., Millán, R., and Franquelo, L. (1999). "Self-commissioning for voltage-referenced voltage-fed vector controlled induction motor drives." In *The 25th Annual Conference of the IEEE Industrial Electronics Society*, vol. 3, pp. 1033–1038.

Bertoluzzo, M., Buja, G. S., and Menis, R. (1997). "Inverter voltage drop-free recursive least-squares parameter identification of a PWM induction motor at standstill." In *Proceedings of the IEEE International Symposium on Industrial Electronics 1997*, vol. 2, pp. 649–654.

Bertoluzzo, M., Buja, G. S., and Menis, R. (2001). "Self-commissioning of RFO IM drives: One-test identification of the magnetization characteristic of the motor." *IEEE Transactions on Industry Applications*, **37**(6), pp. 1801–1806.

Blaabjerg, F. and Pedersen, J. K. (1994). "An ideal PWM-VSI inverter using only one current sensor in the DC-link." In *Proceedings of the 5th International Conference on Power Electronics and Variable-Speed Drives*, pp. 458–464.

Bünte, A. and Grotstollen, H. (1993). "Parameter identification of an inverter-fed induction motor at standstill with a correlation method." *Fifth European Conference on Power Electronics and Applications*, **5**, pp. 97–102.

Buja, G. S., Menis, R., and Valla, M. I. (1995). "MRAS identification of the induction motor parameters in PWM inverter drives at standstill." In *Proceedings of the 1995 IEEE IECON 21st International Conference on Industrial Electronics, Control and Instrumentation*, vol. 2, pp. 1041–1047.

Choi, J.-W. and Soul, S.-K. (1994). "New dead time compensation eliminating zero current clamping in voltage-fed PWM inverter." In *Conference Record of the 1994 IEEE Industry Applications Society Annual Meeting*, no. 2-6, pp. 977–984.

Cirrincione, M., Pucci, M., and Vitale, G. (2002). "A least-squares based methodology for estimating the electrical parameters of induction machine at standstill." In *IEEE International Symposium on Industrical Electronics*, vol. 2, pp. 541–547.

Couto, E. B. and de Aguiar, M. L. (1998). "Parameter identification of induction motors using DC step excitation at standstill." In *IEEE International Symposium on Industrial Electronics*, vol. 2, pp. 468–471.

Dell'Aquila, A., Giliberti, V., Lovecchio, F., and Salvatore, L. (1994). "Real-time estimation of induction motor parameters by lse." In *20th International Conference on Industrial Electronics, Control and Instrumentation*, vol. 3, pp. 2127–2131.

do Prado Junior, A., Heerdt, J. A., and Junior, S. I. S. (2002). "Off-line identification of PWM driver induction motors using reference voltages." In *IEEE 2002 28th Annual Conference of the Industrial Electronics Society*, vol. 3, pp. 2057–2062.

Franklin, G. F., Powell, J. D., and Workman, M. L. (1990). *Digital Control of Dynamic Systems*. Addison-Wesley, CA.

Ganji, A. A., Guillaume, P., Pintelon, R., and Lataire, P. (1996). "Identification of the induction motor dynamic and static inductance with regard to saturation." In *Power Electronics and Variable Speed Drives*, no. 429, pp. 42–47.

Garnier, H., Mensler, M., and Richard, A. (2003). "Continuous-time model identification from sampled data: implementation issues and performance evaluation." *International Journal of Control*, **76**(13), pp. 1337–1357.

Garnier, H. and Young, P. (2004). "Time-domain approaches to continuous-time model identification of dynamical systems from sampled data." In *American Control Conference*, vol. 1, pp. 667–672.

Hanselman, D. and Peake, W. (1995). "Eddy-current effects in slot-bound conductors." In *IEE Proceedings Electric Power Applications*, vol. 142, pp. 131–136.

Harnefors, L. (2003). *Control of Variable-Speed Drives*. Applied Signal Processing and Control, Department of Electronics, University of Mälardalen, Västerås, Sweden.

Hägglund, T. and Åström, K. J. (2006). *Advanced PID Control*. The Instrumentation, Systems, and Automation Society, Research Triangle Park, NC.

Holtz, J. (1994). "Pulsewidth modulation for electronic power conversion." In *Proceedings of the IEEE*, vol. 82, pp. 1194–1214.

Holtz, J. (1995). "The representation of AC machine dynamics by complex signal flow graphs." *IEEE Transactions on Industrial Electronics*, **42**(3), pp. 263–271.

IEC (1994). *IEC Standard 60034-1: Rotating Electrical Machines - Part 1: Rating and Performance*. International Electrotechnical Commission.

IEEE (1991). *IEEE Standard Test Procedure for Polyphase Induction Motors and Generators*. No. Std 112-1991, The Institute of Electrical and Electronics Engineers, Inc.

Johansson, R. (1986). "Identification of continuous-time dynamic systems." In *IEEE 25th Conference on Decision and Control*, pp. 1653–1658.

Johansson, R. (1993). *System Modeling and Identification*. Prentice Hall, NJ.

Kerkman, R. J. (1985). "Steady-state and transient analyses of an induction machine with saturation of the magnetizing branch." *IEEE Transactions on Industry Applications*, **21**(1), pp. 226–234.

Klaes, N. R. (1993). "Parameter identification of an induction machine with regard to dependencies on saturation." *IEEE Transactions on Industry Applications*, **29**(6), pp. 1135–1140.

Kreyszig, E. (1999). *Advanced Engineering Mathematics, 8th ed.* John Wiley, Hoboken, NJ.

Krishnan, R. (2001). *Electric Motor Drives: Modeling, Analysis and Control*. Prentice Hall, Upper Saddle River.

Krishnan, R. and Bharadwaj, A. S. (1991). "A review of parameter sensitivity and adaptation in indirect vector controlled induction motor drive systems." *IEEE Transactions on Power Electronics*, **6**(4), pp. 695–703.

Kwon, W. H., Lee, C. H., Youn, K. S., and Cho, G. H. (1994). "Measurement of rotor time constant taking into account magnetizing flux in the induction motor." In *Conference Record of the 1994 IEEE Industry Applications Society Annual Meeting*, vol. 1, pp. 88–92, IEE.

Kwon, Y.-S., Lee, J.-H., Moon, S.-H., Kwon, B.-K., Choi, C.-H., and Seok, J.-K. (2008). "Standstill parameter identification of vector-controlled induction motors using frequency characteristics of rotor bars." *IEEE Industry Applications Society Annual Meeting*, pp. 1–7.

Leggate, D. and Kerkman, R. J. (1997). "Pulse-based dead-time compensator for PWM voltage inverters." *IEEE Transactions on Industrial Electronics*, **44**(2), pp. 191–197.

Levi, E., Sokola, M., Boglietti, A., and Pastorelli, M. (1996). "Iron loss in rotor-flux-oriented induction machines: identification, assessment of detuning, and compensation." *IEEE Transactions on Power Electronics*, **11**(5).

Ljung, L. (1987). *System identification: theory for the user*. Prentice Hall, NJ, United States.

Ljung, L. and Söderström, T. (1983). *Theory and Practice of Recursive Identification*. MIT Press, MA, United States.

Martin, F. (1996). *Semikron Power Electronics Catalogue*. Semikron International, Nürnberg, Germany.

Melkebeek, J. A. A. and Novotny, D. W. (1983). "The influence of saturation on induction machine drive dynamics." *IEEE Transactions on Industry Applications*, **19**(5), pp. 671–681.

Meyer, C. D. (2000). *Matrix Analysis and Applied Linear Algebra*. Society for Industrial and Applied Mathematics, Philadelphia, PA.

Michalik, W. (1998). "Standstill estimation of electrical parameters in motors with optimal input signals." In *Second IEEE International Caracas Conference on Devices, Circuits and Systems*, pp. 407–413.

Minami, K., Vélez-Reyes, M., Elten, D., Verghese, G. C., and Filbert, D. (1991). "Multi-stage speed and parameter estimation for induction machines." In *22nd Annual IEEE Power Electronics Specialists Conference Record*, no. 24-27, pp. 596–604.

Mohan, N., Undeland, T. M., and Robbins, W. P. (2003). *Power Electronics: Converters, Applications and Design, 3rd ed.* John Wiley, Hoboken, NJ.

Moon, S. and Keyhani, A. (1993). "Estimation of induction machine parameters from standstill time domain data." *Conference Record of the 1993 IEEE Industry Application Society Annual Meeting*, **1**(3-8), pp. 336–342.

Muñoz, A. R. and Lipo, T. A. (1999). "On-line dead-time compensation technique for open-loop PWM-VSI drives." *IEEE Transactions on Power Electronics*, **14**(4), pp. 683–689.

Niiranen, J. (1999). *Sähkömoottorikäytön digitaalinen ohjaus (Digital Control of Electric Motor Drives), 2nd ed.* Otatieto, Helsinki, Finland.

Rasmussen, H., Knudsen, M., and Tønnes, M. (1996). "Parameter estimation of inverter and motor model at standstill using measured currents only." In *Proceedings of the IEEE International Symposium on Industrial Electronics*, vol. 1, pp. 331–336.

Rowan, T., Kerkman, R., and Leggate, D. (1989). "A simple on-line adaptation for indirect field orientation of an induction machine." In *Conference Record of the 1989 IEEE Industry Applications Society Annual Meeting*, vol. 1, pp. 579–587.

Ruff, M. and Grotstollen, H. (1996). "Off-line identification of the electrical parameters of an industrial servo drive system." *Conference Record of the 1996 IEEE Industry Applications*, **1**(6-10), pp. 213–220.

Sadarangani, C. (2000). *Electrical Machines - Design and Analysis of Induction and Permanent Magnet Motors*. US-AB, Stockholm, Sweden.

Salomäki, J. (2003). *Suppression of mechanical vibrations in speed controlled elevator drives*. Master's thesis, Helsinki University of Technology, Finland.

Seok, J.-K., Moon, S.-I., and Sul, S.-K. (1997). "Induction machine parameter identification using PWM inverter at standstill." *IEEE Transactions on Energy Conversion*, **12**(2), pp. 127–132.

Shaw, S. R. and Leeb, S. B. (1999). "Identification of induction motor parameters from transient stator current measurements." *IEEE Transactions on Industrial Electronics*, **46**(1), pp. 139–149.

Slemon, G. R. (1989). "Modelling of induction machines for electric drives." *IEEE Transactions on Industry Applications*, **25**(6), pp. 1126–1131.

Smith, S. W. (2003). *Digital Signal Processing: A Practical Guide for Engineers and Scientists*. Newnes, Burlington, MA.

Sonnaillon, M., Bisheimer, G., Angelo, C. D., and Garcia, G. (2007). "Automatic induction machine parameters measurement using standstill frequency-domain tests." *IET Electronic Power Applications*, **1**(5), pp. 833–838.

Stolt, L. (2005). *Speed Sensorless Control of Squirrel Cage Induction Motors in Elevator Applications*. Master's thesis, Helsinki University of Technology, Finland.

Sukhapap, C. and Sangwongwanich, S. (2002). "Auto tuning of parameters and magnetization curve of an induction motor at standstill." In *IEEE International Conference on Industrial Technology*, vol. 1, pp. 101–106.

Toliyat, H. A., Levi, E., and Raina, M. (2003). "A review of RFO induction motor parameter estimation techniques." *IEEE Transactions on Energy Conversion*, **18**(2), pp. 271–283.

Urasaki, N., Senjyu, T., Uezato, K., and Funabashi, T. (2005). "An adaptive dead-time compensation strategy for voltage source inverter fed motor drives." *IEEE Transactions on Power Electronics*, **20**(5), pp. 1150–1160.

Vas, P. (1993). *Parameter Estimation, Condition Monitoring, and Diagnosis of Electrical Machines*. Clarendon Press, Oxford.

Wang, C., Novotny, D. W., and Lipo, T. A. (1988). "An automated rotor time constant measurement system for indirect field-oriented drives." *IEEE Transactions on Industry Applications*, **24**(1), pp. 151–159.

White, T. and Hinton, J. (1995). "Compensation for the skin effect in vector-controlled induction motor drive systems." In *Electrical Machines and Drives, 1995. Seventh International Conference on (Conf. Publ. No. 412)*, pp. 301–305.

Ylén, J.-P. (2008). *Luentomonisteet tietokonemallintamisesta (Lecture notes in Computer modeling)*. Helsinki University of Technology.

Appendix A: Linear Regression

A system, whose output equation is, for example, an nth order polynomial,

$$y(t) = \theta_0 + \theta_1 u(t) + \ldots + \theta_n u^n(t) \tag{A1}$$

can be written in a matrix form

$$y(t) = \begin{bmatrix} 1 & u(t) & \ldots & u^n(t) \end{bmatrix} \begin{bmatrix} \theta_0 \\ \theta_1 \\ \vdots \\ \theta_n \end{bmatrix} = \boldsymbol{\varphi}^T \boldsymbol{\theta}. \tag{A2}$$

The model parameters θ_i can be solved with linear regression. First, a data set of N measurement points is gathered from the system input $u(t = kh)$ and output $y(t = kh)$ with a sampling period h. Then, the measurements are put into an output vector $\mathbf{Y}$ and a regressor matrix $\boldsymbol{\Phi}$

$$\mathbf{Y} = \begin{bmatrix} y(k_1) \\ y(k_2) \\ \vdots \\ y(N) \end{bmatrix}, \qquad \boldsymbol{\Phi} = \begin{bmatrix} \boldsymbol{\varphi}^T(k_1) \\ \boldsymbol{\varphi}^T(k_2) \\ \vdots \\ \boldsymbol{\varphi}^T(N) \end{bmatrix} = \begin{bmatrix} 1 & u(k_1) & \ldots & u^n(k_1) \\ 1 & u(k_2) & \ldots & u^n(k_2) \\ \vdots & \vdots & \ddots & \vdots \\ 1 & u(N) & \ldots & u^n(N) \end{bmatrix}. \tag{A3}$$

The measurements describe the original system with a matrix equation

$$\mathbf{Y} = \boldsymbol{\Phi}\widehat{\boldsymbol{\theta}} + \mathbf{e} \tag{A4}$$

where the vector $\mathbf{e}^T = \begin{bmatrix} e(k_1) & e(k_2) & \cdots & e(N) \end{bmatrix}$ contains errors between the measurements and the model.

The object is to find a parameter vector $\widehat{\boldsymbol{\theta}}$ describing the real system output as closely as possible. This vector can be found by minimizing the square of errors

$$J(\widehat{\boldsymbol{\theta}}) = \frac{1}{2}\sum_{i=1}^{N} e_i^2 = \frac{1}{2}\mathbf{e}^T\mathbf{e}, \quad \mathbf{e} = \mathbf{Y} - \widehat{\mathbf{Y}} = \mathbf{Y} - \boldsymbol{\Phi}\widehat{\boldsymbol{\theta}} \tag{A5}$$

which can be done with the least-squares (LS) estimate

$$\widehat{\boldsymbol{\theta}} = \left(\boldsymbol{\Phi}^T\boldsymbol{\Phi}\right)^{-1}\boldsymbol{\Phi}^T\mathbf{Y} = \boldsymbol{\Phi}^{\dagger}\boldsymbol{\Phi}^T\mathbf{Y}. \tag{A6}$$

As this involves calculating a time-consuming pseudo-inverse $\boldsymbol{\Phi}^{\dagger}$ of an $N \times N$ matrix, which might have bad numerical properties, it is better to use a recursive version of the least-squares (RLS) estimate

$$\widehat{\boldsymbol{\theta}}(0) = \boldsymbol{\Phi}(0)^{-1}\mathbf{Y}(0) \qquad \text{or} \quad \widehat{\boldsymbol{\theta}}(0) = \mathbf{0}_{n\times 1} \tag{A7a}$$

$$\mathbf{P}(0) = \left(\boldsymbol{\Phi}^T(0)\boldsymbol{\Phi}(0)\right)^{-1} \quad \text{or} \quad \mathbf{P}(0) = \alpha\mathbf{I}_{n\times n} \tag{A7b}$$

$$\boldsymbol{\gamma}(N) = \frac{\mathbf{P}(N)\boldsymbol{\varphi}(N+1)}{\boldsymbol{\varphi}^T(N+1)\mathbf{P}(N)\boldsymbol{\varphi}(N+1) + \mu} \tag{A7c}$$

$$\widehat{\boldsymbol{\theta}}(N+1) = \widehat{\boldsymbol{\theta}}(N) + \boldsymbol{\gamma}(N)\left(y(N+1) - \boldsymbol{\varphi}^T(N+1)\widehat{\boldsymbol{\theta}}(N)\right) \tag{A7d}$$

$$\mathbf{P}(N+1) = \frac{1}{\mu}\left(\mathbf{I} - \boldsymbol{\gamma}(N)\boldsymbol{\varphi}^T(N+1)\right)\mathbf{P}(N+1) \tag{A7e}$$

where $\mathbf{P}$ is the covariance matrix and $\boldsymbol{\gamma}$ the update coefficient. The coefficient α is the covariance matrix gain. The coefficient μ is called forgetting factor, and it is used to weigh newer values more than the old ones. According to Johansson (1993), the RLS estimate uses roughly N previous data points if the coefficient μ is chosen as

$$\mu = \frac{N-1}{N}. \tag{A8}$$

Usually the value is chosen between 0.95 and 0.995. If the value is chosen as unity, the RLS method has no memory, and the obtained parameter vector is the same as if it were calculated using the regular least-squares method.

The RLS method converges rapidly if there is some *a priori* knowledge about the parameters $\boldsymbol{\theta}$ and the covariance matrix $\mathbf{P}$, which means that an $n \times n$ system $\widehat{\boldsymbol{\theta}} = \boldsymbol{\Phi}^{-1}\mathbf{Y}$ should be solved in advance. However, such a process can be an enormous task if the system has more than three parameters ($n > 3$) as it involves inverting an $n \times n$ matrix, which is known to be slow and difficult to do even with proper matrix libraries. In such a case, the parameter vector and the covariance matrix can be initialized to zero, in which case the covariance matrix gain α should be chosen large, i.e. $\alpha \in [10...10000]$. Unfortunately, doing so might cause high initial transients in the parameter estimates.

Even though the least-squares method is fast and accurate, it gives biased results if colored noise enters the input and output signals. This error can be minimized with trend elimination by removing the average from the input and output vectors

$$\mathbf{U} := \mathbf{U} - \frac{1}{N}\sum_{i=1}^{N} u_i \tag{A9a}$$

$$\mathbf{Y} := \mathbf{Y} - \frac{1}{N}\sum_{i=1}^{N} y_i. \tag{A9b}$$

Other methods, which avoid biasing, are the instrumental variable method and the maximum likelihood method. These methods are much more complex and harder to use than the least-squares method. More on linear regression and recursive algorithms can be found in (Ljung and Söderström, 1983), (Ljung, 1987), (Johansson, 1993) and (Ylén, 2008).